Steel 8622 (8822 Low Side) Quenched Core (Atm.) Iteration #100 and 104

Monotonic Tensile and Fatigue Test Results Including Overload Tests

Prepared by:

J. Lindsey
and
A. Fatemi

Department of Mechanical, Industrial and
Manufacturing Engineering
The University of Toledo
Toledo, Ohio 43606

Prepared for:
The AISI Bar Steel Applications Group

September 2009

American
Iron and Steel
Institute

American Iron and Steel Institute
2000 Town Center, Suite 320
Southfield, Michigan 48075
tel: 248-945-4777
fax: 248-352-1740
www.autosteel.org

TABLE OF CONTENTS

NOMENCLATURE

A_o, A_f	initial, final area	S	engineering stress
HB, HRB, HRC	Brinell, Rockwell B-Scale, Rockwell C-Scale Hardness number	YS, UYS, LYS, YS'	Monotonic yield, upper yield, lower yield, cyclic yield strength
b, c, n	fatigue strength, fatigue ductility, strain hardening exponent	YPE	yield point elongation
D_o, D_f	initial, final diameter	S_u	ultimate tensile strength
e	engineering strain	%EL	percent elongation
E, E'	monotonic, midlife cycle modulus of elasticity	%RA	percent reduction in area
K, K'	monotonic, cyclic strength coefficient	σ, σ_f, σ_f'	true stress, true fracture strength, fatigue strength coefficient
L_o, L_f	initial, final gage length	σ_a, σ_m, $\Delta\sigma$	stress amplitude, mean stress, stress range
$N_{50\%}$, $(N_f)_{10\%}$, $(N_f)_{50\%}$,	number of cycles to midlife, 10% load drop, 50% load drop,	ε_e, ε_p, ε	true elastic, plastic, total strain
$2N_f$	reversals to failure	ε_f, ε_f'	true fracture ductility, fatigue ductility coefficient
P_f, P_u	fracture, ultimate load	ε_a, ε_m, $\Delta\varepsilon$	strain amplitude, mean strain, strain range
R	strain ratio, neck radius	$\Delta\varepsilon_e$, $\Delta\varepsilon_p$	elastic, plastic strain range

NOMENCLATURE

$\sigma_{m,\,SC}$	small cycle mean stress,	$\sigma_{a,\,SC}$	small cycle stress amplitude,
$\sigma_{m,\,OL}$	overload cycle mean stress	$\sigma_{a,\,OL}$	overload cycle stress amplitude
$\varepsilon_{a,\,SC}$	small cycle strain amplitude	$(\Delta\varepsilon_p/2)_{SC}$	small cycle plastic strain amplitude,
$\varepsilon_{a,\,OL}$	overload cycle strain amplitude	$(\Delta\varepsilon_p/2)_{OL}$	overload plastic strain amplitude
$\varepsilon_{m,\,SC}$	small cycle mean strain	B, B_f	number of blocks in a periodic overload test, number of blocks to failure in a periodic overload test
N_{SC}, $N_{f,\,SC(eq)}$	number of small cycles in an overload block, calculated equivalent life of the small cycles in an overload test	$N_{f,\,OL}$	Constant amplitude life to failure at the strain amplitude used for the periodic overload cycle amplitude

UNIT CONVERSION TABLE

Measure	SI Unit	US Unit	from SI to US	from US to SI
Length	mm	in	1 mm = 0.03937 in	1 in = 25.4 mm
Area	mm^2	in^2	1 mm^2 = 0.00155 in^2	1 in^2 = 645.16 mm^2
Load	kN	klb	1kN = 0.2248 klb	1 klb = 4.448 kN
Stress	MPa	ksi	1 MPa = 0.14503 ksi	1 ksi = 6.895 MPa
Temperature	^oC	^oF	$^oC = (^oF - 32)/1.8$	$^oF = (^oC * 1.8) + 32$

In SI Unit:	1 kN = 10^3 N	1 Pa = 1 N/m^2	1 MPa = 10^6 Pa = 1 N/mm^2	1 Gpa = 10^9 Pa
In US Unit:	1 klb = 10^3 lb	1 psi = 1 lb/in^2	1 ksi = 10^3 psi	

SUMMARY

Monotonic tensile properties and fatigue behavior data were obtained for steel material of iterations 100 and 104. The material was provided by AISI. Two tensile tests were performed to acquire the desired monotonic properties. Both tests gave similar results. Twenty strain-controlled fatigue tests were performed to obtain the fatigue life and cyclic deformation curves and properties. The experimental procedure followed and results obtained are presented and discussed in this report. Periodic overload fatigue behavior and data were also obtained from twelve strain-controlled periodic overload fatigue tests. The experimental procedure followed and results obtained from periodic overload tests are also presented and discussed in this report.

I. EXPERIMENTAL PROGRAM

1.1 Material and Specimen Fabrication

1.1.1 Material

The steel material was provided by AISI. The test specimen was prepared from an 8822 steel grade with low side chemistry. The samples were quenched and tempered by austenitizing at 1700F prior to quenching in 150F oil and then tempering at 1050F to an aim hardness of 25-30 HRC (see Appendix B). Inclusion distribution and microstructure of the material are shown in Figures 1 and 2, respectively.

1.1.2 Specimen

In this study, identical round specimens were used for monotonic and fatigue tests. The specimen configuration and dimensions are shown in Figure 3. This configuration deviates slightly from the specimens recommended by ASTM Standard E606 [1]. The recommended specimens have uniform gage sections. The specimen geometry shown in Figure 3 differs by using a large secondary radius in the gage section to compensate for the slight stress concentration at the gage to grip section transition.

All specimens were machined in the Mechanical, Industrial, and Manufacturing Engineering Machine Shop at the University of Toledo. The specimens were initially turned on a lathe to an appropriate diameter for insertion into a CNC/milling machine. Using the CNC machine, final turning was performed to achieve the tolerable dimensions specified on the specimen drawings.

The specimens were then polished prior to testing at the University of Toledo. A commercial round-specimen polishing machine was used to polish the specimen gage section. Three different grits of aluminum oxide lapping film 30 μm, 12 μm, and 3 μm were used. Polishing marks coincided with the longitudinal direction of the specimen. The polished surfaces were carefully examined under magnification to ensure complete removal of machine marks within the test section.

1.2 Testing Equipment

1.2.1 Apparatus

An INSTRON 8801 closed-loop servo-controlled hydraulic axial load frame in conjunction with a Fast-Track digital servo-controller was used to conduct the tests. The load cell used had a capacity of 50 kN. Hydraulically operated grips using universal tapered collets were employed to secure the specimens' ends in series with the load cell.

Total strain was controlled using an extensometer rated as ASTM class B1 [2]. The calibration of the extensometer was verified using displacement apparatus containing a micrometer barrel in divisions of 0.0001 in. The extensometer had a gage length of 0.30 in. and was capable of measuring strains up to 15 %.

In order to protect the specimens' surface from the knife-edges of the extensometer, ASTM Standard E606 recommends the use of transparent tape or epoxy to 'cushion' the attachment. For this study, it was found that application of transparent tape strips was difficult due to the size of the test section. Therefore, epoxy was considered to be the best protection. The tests were performed using M-coat D.

1.2.2 Alignment

Significant effort was put forth to align the load train (load cell, grips, specimen, and actuator). Misalignment can result from both tilt and offset between the central lines of the load train components. In order to align the machine, a round strain-gage bar with two arrays of four strain gages per array that were arranged at the upper and lower ends of the uniform gage section was used. This was done in accordance with ASTM Standard E1012 [3].

1.3 Test Methods and Procedures

1.3.1 Monotonic tension tests

Monotonic tests in this study were performed using test methods specified by ASTM Standard E8 [4]. Two specimens were used to obtain the monotonic properties.

In order to protect the extensometer, strain control was used only up to 10% strain, until the point of ultimate tensile strength had been crossed. After this point, displacement control was used until fracture. INSTRON Bluehill software was used for the monotonic tests. For the elastic and initial yield region (0% to 0.5% strain) as well as the period up to which the extensometer was removed, a strain rate of 0.0025 in/in/min was chosen. This strain rate was three-quarters of the maximum allowable rate specified by ASTM Standard E8 for the initial yield region. After the extensometer was removed, a displacement rate of 0.006 in/min was used.

After the tension tests were concluded, the broken specimens were carefully reassembled. The final gage lengths of the fractured specimens were measured with a

Vernier caliper having divisions of 0.001 in. Using an optical comparator with 10X magnification and divisions of 0.001 in, the final diameter and neck radius were measured. It should be noted that prior to the test, the initial diameter was measured with this same instrument.

1.3.2 Constant amplitude fatigue tests

All constant amplitude fatigue tests in this study were performed according to ASTM Standard E606. It is recommended by this standard that at least 10 specimens be used to generate the fatigue properties. For this study, 20 specimens at 7 different strain amplitudes ranging from 0.250% to 2.000% were utilized. INSTRON LCF software was used in all strain-controlled tests. During each strain-controlled test, the total strain was recorded using the extensometer output. Test data were automatically recorded throughout each test.

There were two control modes used for these tests. Strain control was used in all tests with plastic deformation. For one of the elastic tests, strain control was used initially to determine the stabilized load, then load control was used for the remainder of the test and for the rest of the elastic tests, load control was used throughout. The reason for the change in control mode was due to the frequency limitation on the extensometer. For the strain-controlled tests, the applied frequencies ranged from 0.2 Hz to 5 Hz in order to keep a strain rate about 0.02 in/in/sec. For the load-controlled tests, load waveforms with frequencies of up to 25 Hz were used in order to shorten the overall test duration. All tests were conducted using a triangular waveform except the tests run at 25 Hz, when a sinusoidal waveform was used.

1.3.3 Periodic overload fatigue tests

The overload tests were conducted to investigate the effects of periodic overloads on the fatigue life of smaller subsequent cycles. For this study, 12 specimens were tested at 8 different strain amplitudes. The periodic overload tests were run in strain-control with INSTRON WAVERUNNER software. During each strain-controlled test, the total strain was recorded using the extensometer output. Test data were automatically recorded throughout each test

The input signal consisted of a periodic fully reversed overload of the type shown in Figure 13. The load history in these tests consisted of repeated load blocks made up of one fully-reversed overload cycle followed by a group of smaller constant amplitude cycles having the same maximum stress as the overload cycle. The overload cycles were applied at frequent intervals to maintain a low crack opening stress resulting in the subsequent cycles being fully open.

With this overload history, as the large cycles become more frequent, the fraction of the total damage done by them increases and that done by the small cycles decreases. The fully reversed strain amplitude for the overload cycle corresponded to 10^4 cycles to failure. The number of small cycles per block, N_{sc}, were adjusted so that they cause 80 to 90% of the damage per block. Small cycle strain levels were selected at or below the run out level of the constant amplitude tests. Small cycles strain amplitudes were used from 0.275% to 0.075% and the number of small cycles per overload cycle ranged between 100 and 1000.

II. Experimental results and analysis

2.1 Microstructural Data

A specimen was sectioned longitudinally from the grip end and transversely from the gage section to obtain a general microstructure description. The sample was prepared with standard test procedures for sectioning, mounting, polishing, and etched with 3% nital. The sample was reviewed and microphotographs were taken using an Olympus PMG3 Microscope. The microphotographs revealed that the entire sample consisted of tempered martensite. There is some evidence of banding in the longitudinal section from the grip end (see Appendix B). The chemistry of the material is presented in Table 1. Figure 1 shows a photo of the inclusion distribution in the steel and Figure 2 shows a high magnification view of the microstructure from the gage area. The complete material report for this steel was provided by the Chrysler Materials Engineering Lab and is attached as Appendix B of this report.

2.2 Monotonic Deformation Behavior

The properties determined from monotonic tests were the following: modulus of elasticity (E), yield strength (YS), ultimate tensile strength (S_u), percent elongation (%EL), percent reduction in area (%RA), true fracture strength (σ_f), true fracture ductility (ε_f), strength coefficient (K), and strain hardening exponent (n).

True stress (σ), true strain (ε), and true plastic strain (ε_p) were calculated from engineering stress (S) and engineering strain (e), according to the following relationships which are based on constant volume assumption:

True stress (σ), true strain (ε), and true plastic strain (ε_p) were calculated from engineering stress (S) and engineering strain (e), according to the following relationships which are based on constant volume assumption:

$$\sigma = S(1+e) \tag{1a}$$

$$\varepsilon = \ln(1+e) \tag{1b}$$

$$\varepsilon_p = \varepsilon - \varepsilon_e = \varepsilon - \frac{\sigma}{E} \tag{1c}$$

The true stress (σ) - true strain (ε) plot is often represented by the Ramberg-Osgood equation:

$$\varepsilon = \varepsilon_e + \varepsilon_p = \frac{\sigma}{E} + \left(\frac{\sigma}{K}\right)^{\frac{1}{n}} \tag{2}$$

The strength coefficient, K, and strain hardening exponent, n, are the intercept and slope of the best line fit to true stress (σ) versus true plastic strain (ε_p) data in log-log scale:

$$\sigma = K\left(\varepsilon_p\right)^n \tag{3}$$

In accordance with ASTM Standard E739 [5], when performing the least squares fit, the true plastic strain (ε_p) was the independent variable and the true stress (σ) was the dependent variable. These plots for the two tests conducted are shown in Figure 4. To generate the K and n values, the range of data used in this figure was chosen according to the definition of discontinuous yielding specified in ASTM Standard E646 [6]. Therefore, the valid data range occurred between the end of yield point extension and the strain at maximum load.

The true fracture strength was corrected for necking according to the Bridgman correction factor [7]:

$$\sigma_f = \frac{\frac{P_f}{A_f}}{\left[1+\frac{4R}{D_f}\right]\ln\left[1+\frac{D_f}{4R}\right]} \tag{4}$$

where P_f is load at fracture, R is the neck radius, and D_f is the diameter at fracture.

The true fracture ductility, ε_f, was calculated from the relationship based on constant volume:

$$\varepsilon_f = \ln\left(\frac{A_o}{A_f}\right) = \ln\left(\frac{1}{1-RA}\right) \tag{5}$$

where A_f is the cross-sectional area at fracture, A_o is the original cross-sectional area, and RA is the reduction in area.

A summary of the monotonic properties for this material is provided in Table A.1. The monotonic stress-strain curves are shown in Figure 5. As can be seen from this figure, the two curves are very close to each other. Refer to Table A.1 for a summary of the monotonic test results.

2.3 Cyclic Deformation Behavior

2.3.1 Transient cyclic response

Transient cyclic response describes the process of cyclic-induced change in deformation resistance of a material. Data obtained from constant amplitude strain-controlled fatigue tests were used to determine this response. Plots of stress amplitude variation versus applied number of cycles can indicate the degree of transient cyclic softening/hardening. Also, these plots show when cyclic stabilization occurs. A composite plot of the transient cyclic response for the steel studied is shown in Figure A.1. The transient response was normalized on the rectangular plot in Figure A.1a, while a semi-log plot is shown in Figure A.1b. Even though multiple tests were conducted at each strain amplitude, data from one test at each strain amplitude tested are shown in these plots.

2.3.2 Steady-state cyclic deformation

Another cyclic behavior of interest was the steady state or stable response. Data obtained from constant amplitude strain-controlled fatigue tests were also used to determine this response. The properties determined from the steady-state hysteresis loops were the following: cyclic modulus of elasticity (E'), cyclic strength coefficient (K'), cyclic strain hardening exponent (n'), and cyclic yield strength (YS'). Half-life (midlife) hysteresis loops and data were used to obtain the stable cyclic properties.

Similar to monotonic behavior, the cyclic true stress-strain behavior can be characterized by the Ramberg-Osgood type equation:

$$\frac{\Delta \varepsilon}{2} = \frac{\Delta \varepsilon_e}{2} + \frac{\Delta \varepsilon_p}{2} = \frac{\Delta \sigma}{2E} + \left(\frac{\Delta \sigma}{2K'}\right)^{\frac{1}{n'}} \qquad (6)$$

It should be noted that in Equation 6 and the other equations that follow, E is the average modulus of elasticity that was calculated from the monotonic tests.

The cyclic strength coefficient, K', and cyclic strain hardening exponent, n', are the intercept and slope of the best line fit to true stress amplitude ($\Delta\sigma/2$) versus true plastic strain amplitude ($\Delta\varepsilon_p/2$) data in log-log scale:

$$\frac{\Delta\sigma}{2} = K'\left(\frac{\Delta\varepsilon_p}{2}\right)^{n'} \tag{7}$$

In accordance with ASTM Standard E739 [5], when performing the least squares fit, the true plastic strain amplitude ($\Delta\varepsilon_p/2$) was the independent variable and the stress amplitude ($\Delta\sigma/2$) was the dependent variable. The true plastic strain amplitude was calculated by the following equation:

$$\frac{\Delta\varepsilon_p}{2} = \frac{\Delta\varepsilon}{2} - \frac{\Delta\sigma}{2E} \tag{8}$$

This plot is shown in Figure 6. To generate the K' and n' values, the range of data used in this figure was chosen for $\left[\frac{\Delta\varepsilon_p}{2}\right]_{calculated} \geq 0.0001$ in/in.

The cyclic stress-strain curve reflects the resistance of a material to cyclic deformation and can be vastly different from the monotonic stress-strain curve. The cyclic stress-strain curve is shown in Figure 7. In Figure 8, superimposed plots of monotonic and cyclic curves are shown. As can be seen in this figure, the material cyclically softened. Figure A.2 shows a composite plot of the steady-state (midlife) hysteresis loops. Even though multiple tests were conducted at each strain amplitude, the stable loops from only one test at each strain amplitude are shown in this plot.

2.4 Constant Amplitude Fatigue Behavior

Constant amplitude strain-controlled fatigue tests were performed to determine the strain-life curve. The following equation relates the true strain amplitude to the fatigue life:

$$\frac{\Delta\varepsilon}{2}=\frac{\Delta\varepsilon_e}{2}+\frac{\Delta\varepsilon_p}{2}=\frac{\sigma_f'}{E}\left(2N_f\right)^b+\varepsilon_f'\left(2N_f\right)^c \tag{9}$$

where σ_f' is the fatigue strength coefficient, b is the fatigue strength exponent, ε_f' is the fatigue ductility coefficient, c is the fatigue ductility exponent, E is the monotonic modulus of elasticity, and $2N_f$ is the number of reversals to failure.

The fatigue strength coefficient, σ_f', and fatigue strength exponent, b, are the intercept and slope of the best line fit to true stress amplitude ($\Delta\sigma/2$) versus reversals to failure ($2N_f$) data in log-log scale:

$$\frac{\Delta\sigma}{2}=\sigma_f'\left(2N_f\right)^b \tag{10}$$

In accordance with ASTM Standard E739, when performing the least squares fit, the stress amplitude ($\Delta\sigma/2$) was the independent variable and the reversals to failure ($2N_f$) was the dependent variable. This plot is shown in Figure 9. To generate the σ_f' and b values, all data, with the exception of the run-out tests, in the stress-life figure were used.

The fatigue ductility coefficient, ε_f', and fatigue ductility exponent, c, are the intercept and slope of the best line fit to calculated true plastic strain amplitude ($\Delta\varepsilon_p/2$) versus reversals to failure ($2N_f$) data in log-log scale:

$$\left(\frac{\Delta\varepsilon_p}{2}\right)_{calculated}=\varepsilon_f'\left(2N_f\right)^C \tag{11}$$

In accordance with ASTM Standard E739, when performing the least squares fit, the calculated true plastic strain amplitude ($\Delta\varepsilon_p/2$) was the independent variable and the reversals to failure ($2N_f$) was the dependent variable. The calculated true plastic strain amplitude was determined from Equation 8. This plot is shown in Figure 10. To generate the ε_f' and c values, the range of data used in this figure was chosen for

$$\left[\frac{\Delta\varepsilon_p}{2}\right]_{calculated} \geq 0.0001 \text{ in/in.}$$

The true strain amplitude versus reversals to failure plot is shown in Figure 11. This plot displays the strain-life curve (Eqn. 9), the elastic strain portion (Eqn. 10), the plastic strain portion (Eqn. 11), and superimposed fatigue data. A summary of the cyclic properties for this steel is provided in Table 2. Table A.2 provides the summary of the fatigue test results.

A parameter often used to characterize fatigue behavior at stress concentrations, such as at the root of a notch, is Neuber parameter [7]. Neuber's stress range is given by:

$$\sqrt{(\Delta\varepsilon)(\Delta\sigma)E} = 2\sqrt{(\sigma_f')^2(2N_f)^{2b} + \sigma_f'\varepsilon_f'E(2N_f)^{b+c}} \qquad (12)$$

A plot of Neuber stress range versus reversals to failure is shown in Figure 12. This figure displays the Neuber curve based on Eqn. 12 and superimposed fatigue data for this material

2.5 Periodic Overload Fatigue Behavior

Periodic Overload strain-controlled fatigue tests were performed to determine the effective strain-life curve. The effective strain-life curve is plotted using the strain amplitude of the small cycles in the overload block and the calculated equivalent life. The equivalent fatigue lives for the smaller cycles were obtained using the linear damage rule:

$$\frac{N_{OL}}{N_{f,OL}} + \frac{N_{SC}}{N_{f,SC(eq)}} = 1 \qquad (13)$$

where N_{OL} is the number of overload cycles in a periodic overload test, $N_{f,OL}$ is the number of cycles to failure if only overloads were applied in a test, N_{SC} is the number of smaller cycles in a periodic overload test, and $N_{f,SC(eq)}$ is the computed equivalent fatigue life for the smaller cycles.

The linear damage rule was also used to calculate the cumulative damage of the overload cycles, D_{OL}, as

$$\frac{N_{OL}}{N_{f,OL}} = D_{OL} \qquad (14)$$

Figure 14 shows the effective strain-life data superimposed on the constant amplitude strain life plot. Table A.3 presents a summary of the periodic overload test results.

A plot of the SWT parameter for both the constant amplitude and overload data provides another method of comparison between the two sets of data, where the mean stress present in the small cycles is taken into account. The SWT parameter is given by

$$\sigma_{\max}\varepsilon_a = \frac{1}{E}[(\sigma_f')^2(2N_f)^{2b} + \sigma_f'\varepsilon_f'E(2N_f)^{b+c}] \qquad (15)$$

where $\sigma_{\max} = \sigma_m + \sigma_a$. The SWT plot is shown in Figure 15. As in the constant amplitude strain-life curve, the overload data and effective strain-life curve diverged from the constant amplitude curve.

Plots of the overload cycle and small cycle stress amplitude variation versus applied number of blocks can indicate the degree of transient cyclic softening/hardening. Also, these plots show when cyclic stabilization occurs over the life of the specimen. A composite plot of the small cycle transient cyclic response for the steel studied is shown in Figures A.3. A composite plot of the overload cycle transient cyclic response is shown in Figure A.4. The amplitude of the transient response is shown in the Figures A.3a and

A.4a while the mean of the transient response is shown in Figures A.3b and A.4b. Even though multiple tests were conducted at each strain amplitude, data from one test at each strain amplitude tested are shown in these plots. While small cycle stress amplitude was constant during each test (Figure A3.a), there was significant small cycle mean stress relaxation (Figure A3.b). The overload stress amplitude reduced significantly during life (i.e. cyclic softening), while the overload mean stress was near zero (see Figure A.4b), as expected, since the overload cycles were fully reversed.

Stress response of small cycles was also evaluated within a single block. This can be seen in Figure A.5b, which is a plot of the mean stress at each strain level within a single block at midlife and in Figure A.5a, which shows the stress amplitude at each strain level within a single block at midlife. Once again, although multiple tests were conducted at each strain amplitude, data from one test at each strain amplitude tested are shown in these plots. These plots show steady state stress response within a load block.

The midlife hysteresis loops for each small cycle strain level are shown in Figures A.6a through A.6i. The small cycle loop was taken from the mid-cycle of the midlife block.

Table 1: Chemical Composition of 8622 (8822 Low Side) Steel (Courtesy of Chrysler)

Element	**Wt. %**
Carbon, C	0.210%
Manganese, Mn	0.810%
Phosphorus, P	0.020%
Sulfur, S	0.026%
Silicon, Si	0.260%
Chromium, Cr	0.500%
Aluminum, Al	0.031%
Nickel, Ni	0.460%
Molybdenum, Mo	0.250%
Copper, Cu	0.180%
Tin, Sn	0.010%
Vanadium, V	0.005%
Niobium, Nb	0.002%
DI	2.260%

Table 2: Summary of the Mechanical Properties

Microstructural Data	Average
ASTM grain size number (MAG=500X):	
First longitudinal direction (L-T)	Fine grain 5 - 8
Inclusion rating number (MAG=100x): (Provided by Macsteel Company)	
Type A (sulfide type), thin series	-
Type B (alumina type), thin & heavy series	-
Type C (silicate type, thin & heavy series	-
Type D (globular type), thin & heavy series	-
Hardness:	
Brinell (HB)(converted)	
the longitudinal direction	-
Transverse direction	297
Rockwell B-scale (HRB)	
The first longitudinal direction	-
Transverse direction	-
Rockwell C-scale (HRC)(measured)	
The longitudinal direction	-
Transverse direction	31.5
Microstructure type:	
The longitudinal direction	tempered martensite
Transverse direction	

Monotonic Properties	Average		Range		
Modulus of elasticity, E, GPa (ksi):	211.6	(30,689)	211.6	- 211.6	(30,689) - (30,689)
Yield strength (0.2% offset), YS , MPa (ksi):	883.5	(128.1)	884.2	- 882.8	(128.2 - 128.0)
Upper yield strength UYS, MPa (ksi):	903.6	(131.0)	909.9	- 897.3	(132.0 - 130.1)
Lower yield strength LYS, MPa (ksi):	883.5	(128.1)	884.2	- 882.8	(128.2 - 128.0)
Yield point elongation, YPE (%):	-	-	-	- -	- - -
Ultimate strength, S_u , MPa (ksi):	945.7	(137.2)	947.7	- 943.6	(137.4 - 136.9)
Percent elongation, %EL (%):	36.8%		37.2%	- 36.3%	
Percent reduction in area, %RA (%):	67.2%		67.5%	- 66.9%	
Strength coefficient, K , MPa (ksi):	1,073.5	(155.7)	1,080.7	- 1,066.2	(156.7 - 154.6)
Strain hardening exponent, n:	0.0249		0.0263	- 0.0235	
True fracture strength, σ_f , MPa (ksi):	1170.2	(169.7)	1312.8	- 1027.6	(190.4 - 149.0)
True fracture ductility, ε_f (%):	111.5%		112.3%	- 110.6%	

Cyclic Properties	Average		Range		
Cyclic modulus of elasticity, E' , GPa (ksi):	198.8	(28,836)	206.1	- 192.7	(29,898) - (27,941)
Fatigue strength coefficient, σ_f' , MPa (ksi):	1,094.6	(158.8)			
Fatigue strength exponent, b:	-0.0525				
Fatigue ductility coefficient, ε_f' :	1.097				
Fatigue ductility exponent, c:	-0.6640				
Cyclic strength coefficient, K' , MPa (ksi):	1,153.5	(167.3)			
Cyclic strain hardening exponent, n':	0.0939				
Cyclic yield strength, YS', MPa (ksi)	643.5	(93.3)			
Fatigue Limit (defined at 10^6 cycles), Mpa (ksi)	511.2	(74.1)			

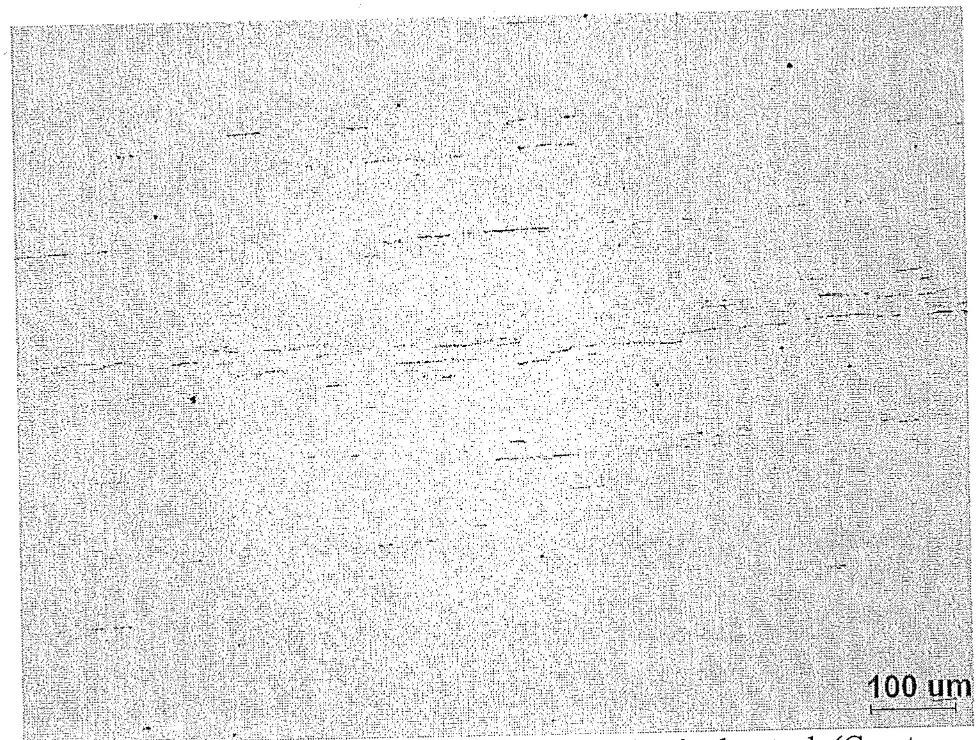

Figure. 1: Micrograph of the inclusion distribution in the steel. (Courtesy of Chyrsler)

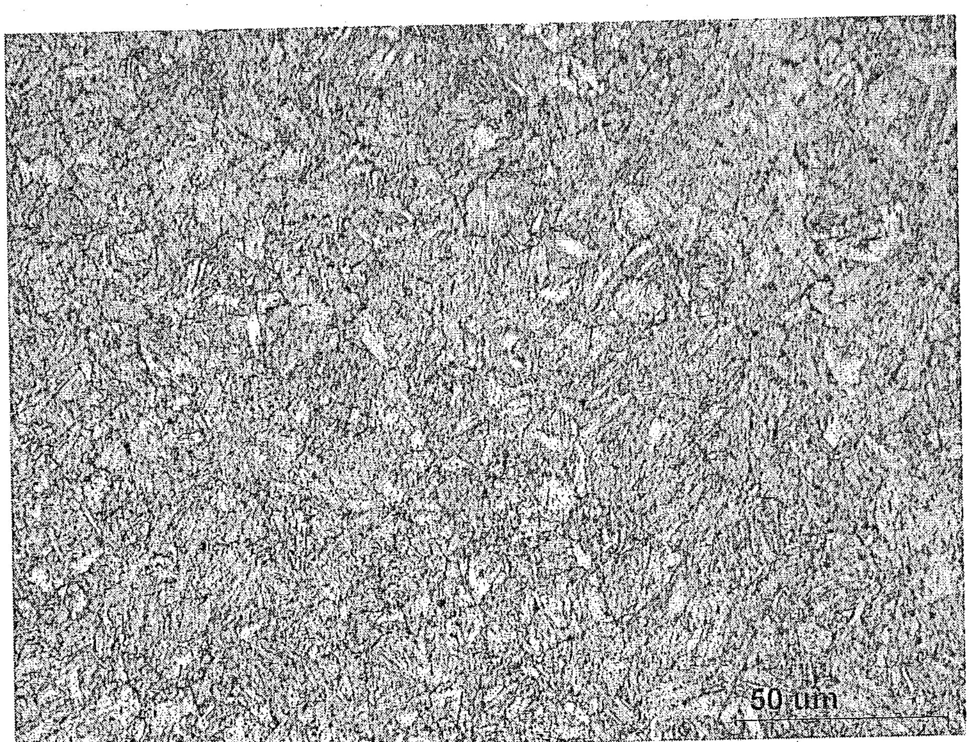

Figure 2: High magnification photo showing the microstructure of the transverse section from the gage area. (Courtesy of Chyrsler)

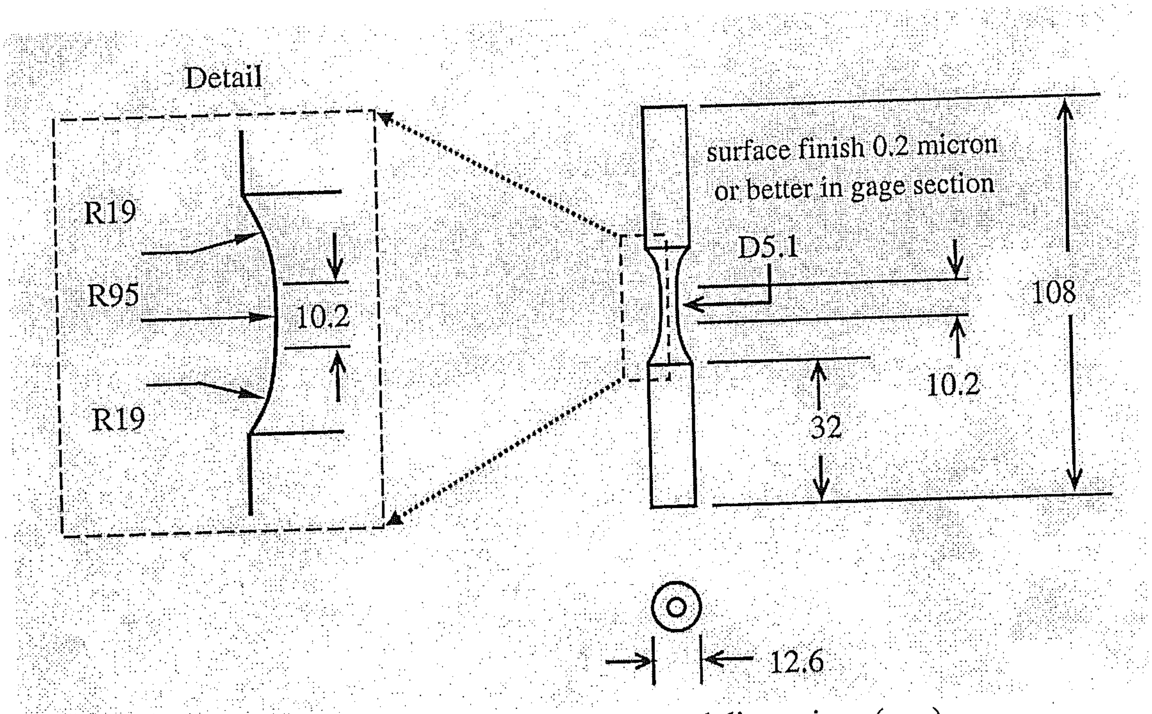

Figure 3: Specimen configuration and dimensions (mm)

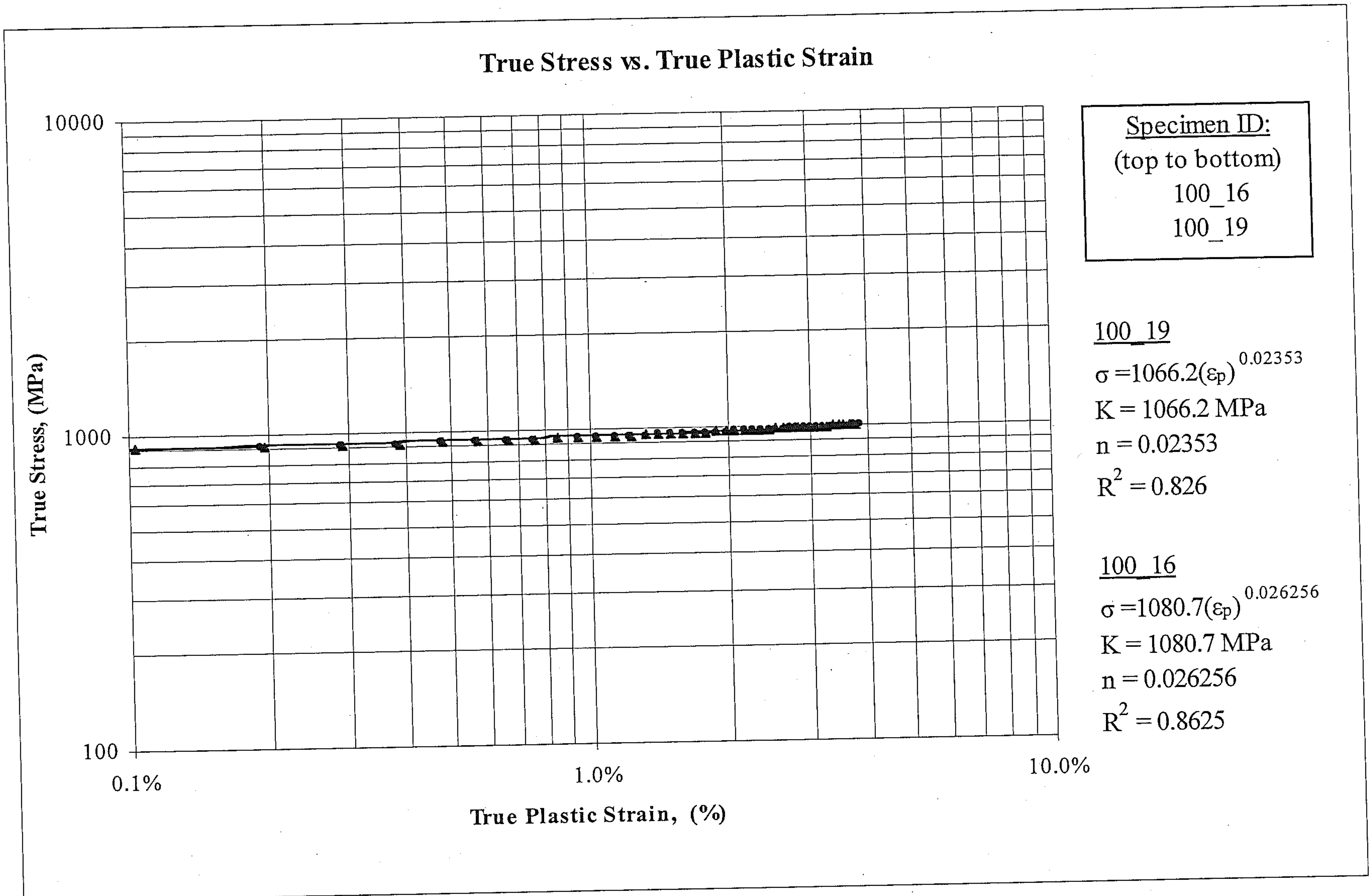

Figure 4: True stress versus true plastic strain

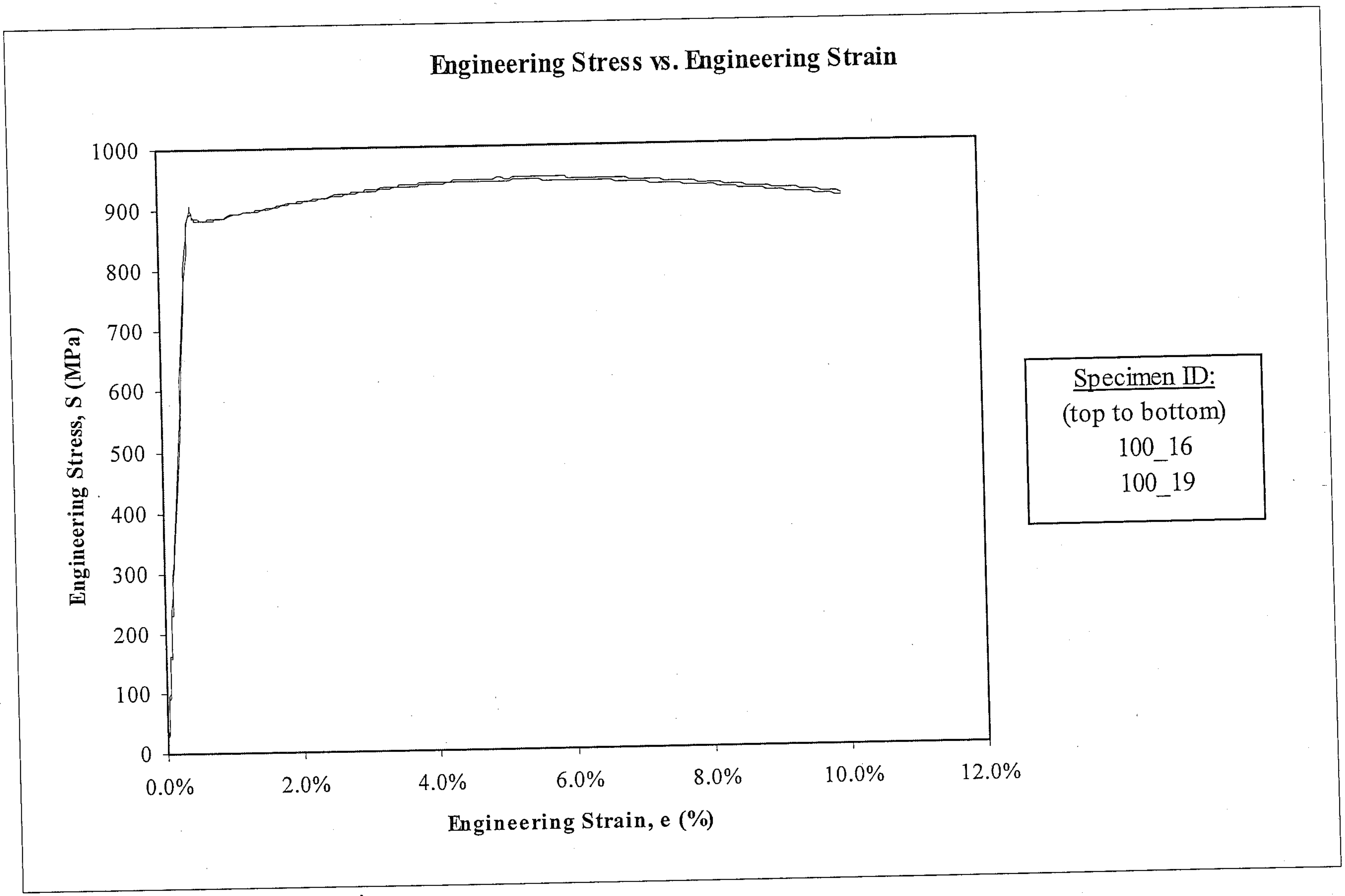

Figure 5: Monotonic stress-strain curves

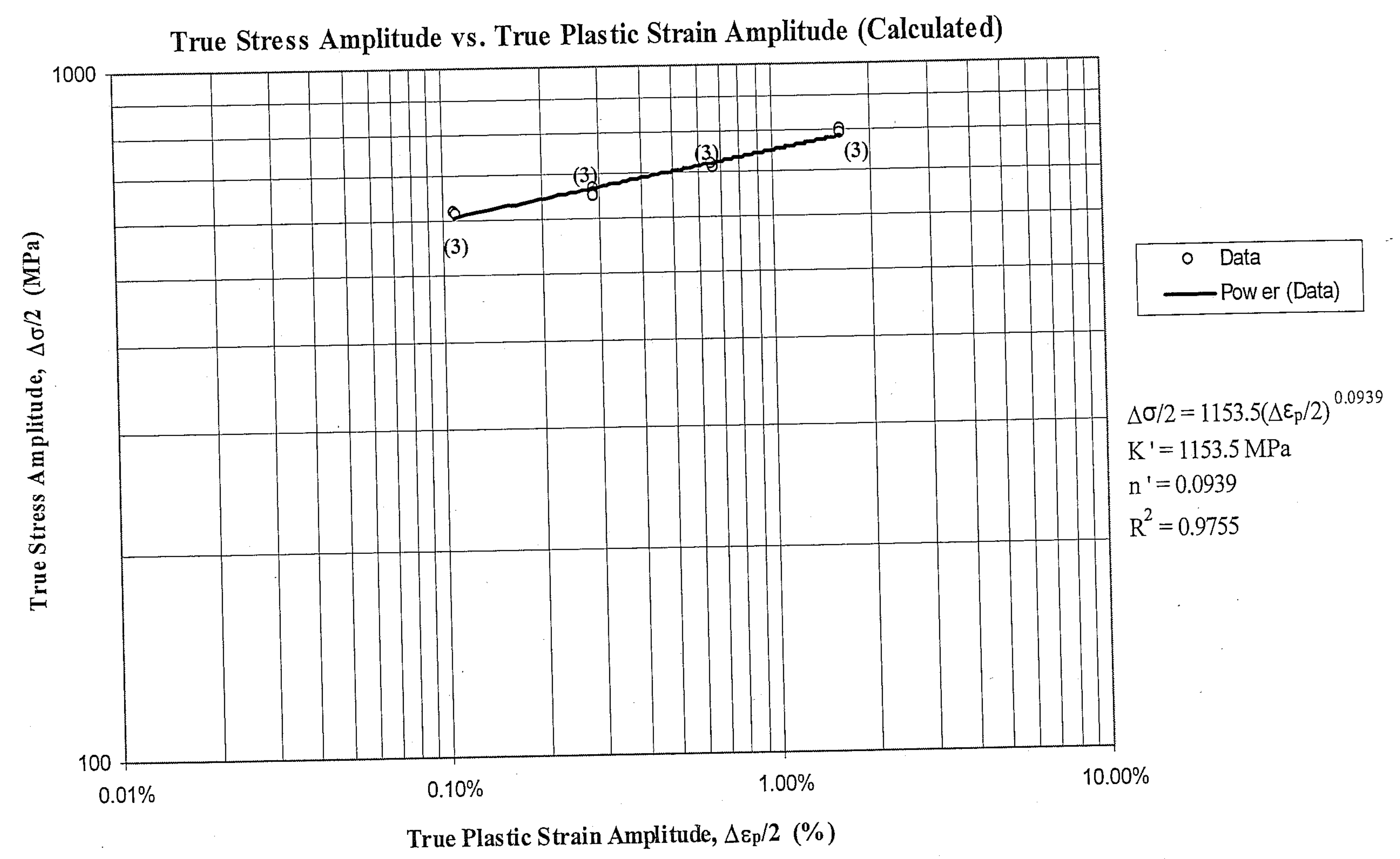

Figure 6: True stress amplitude versus true plastic strain amplitude (calculated)

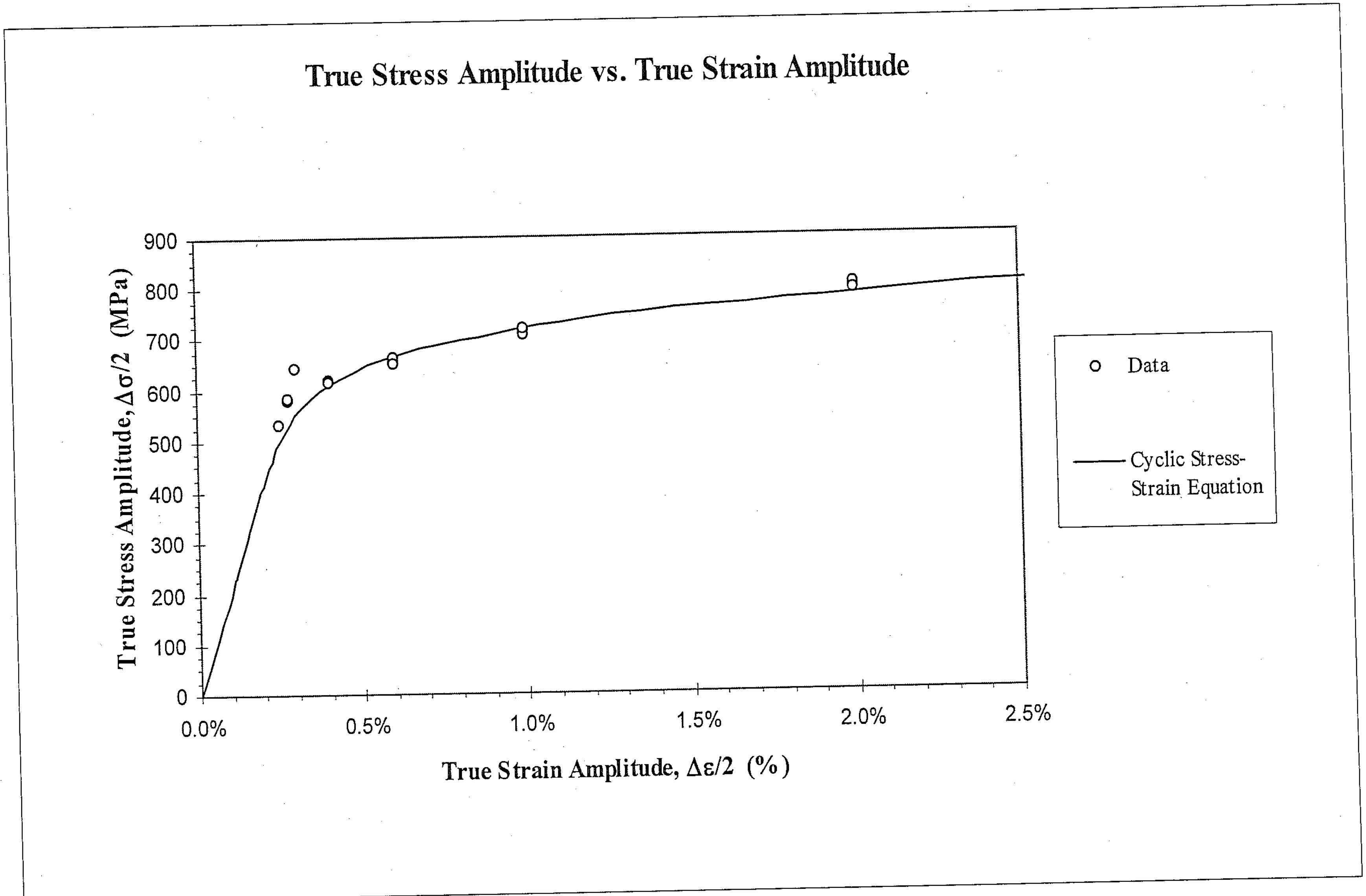

Figure 7: True stress amplitude versus true strain amplitude

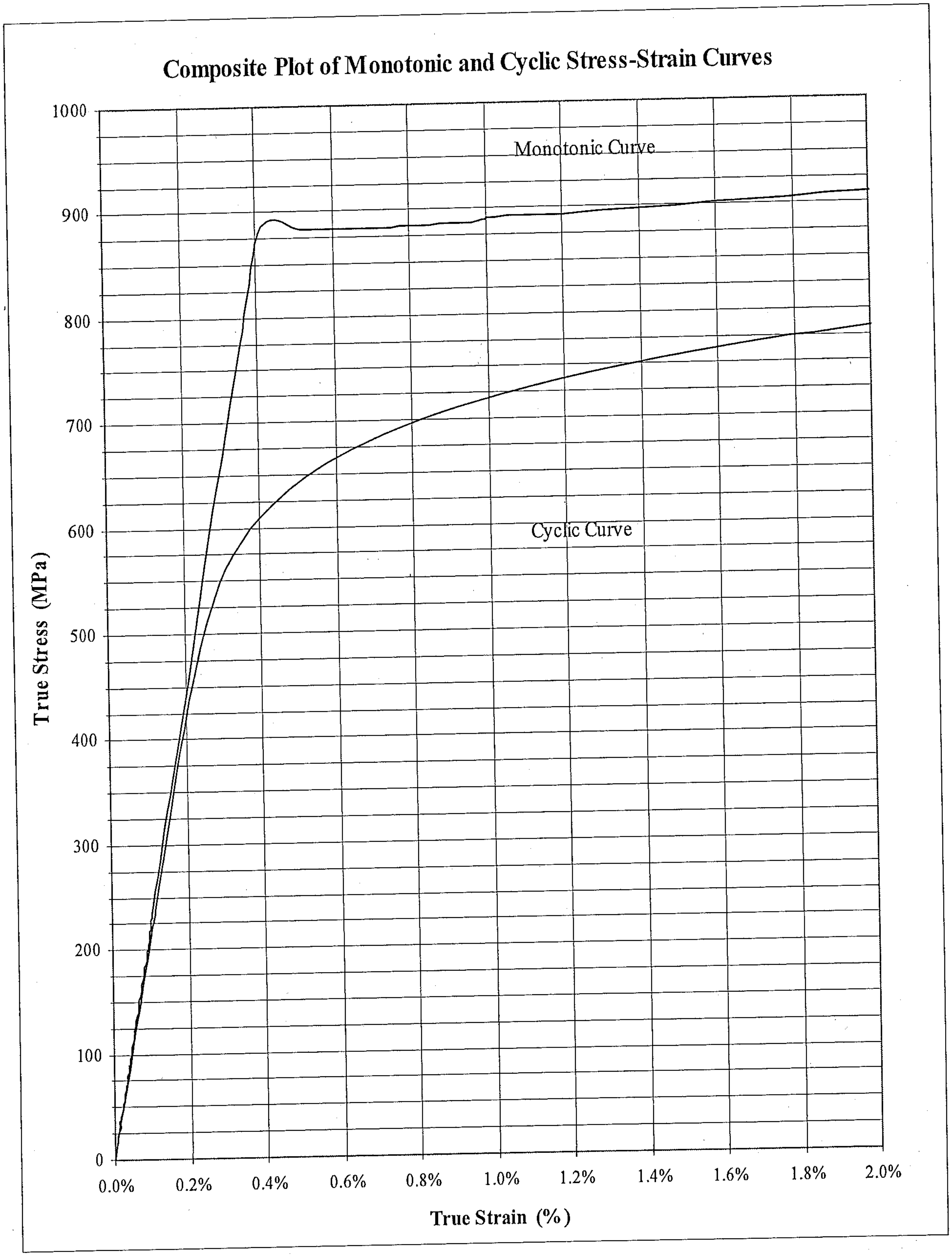

Figure 8: Composite plot of cyclic and monotonic stress-strain curves

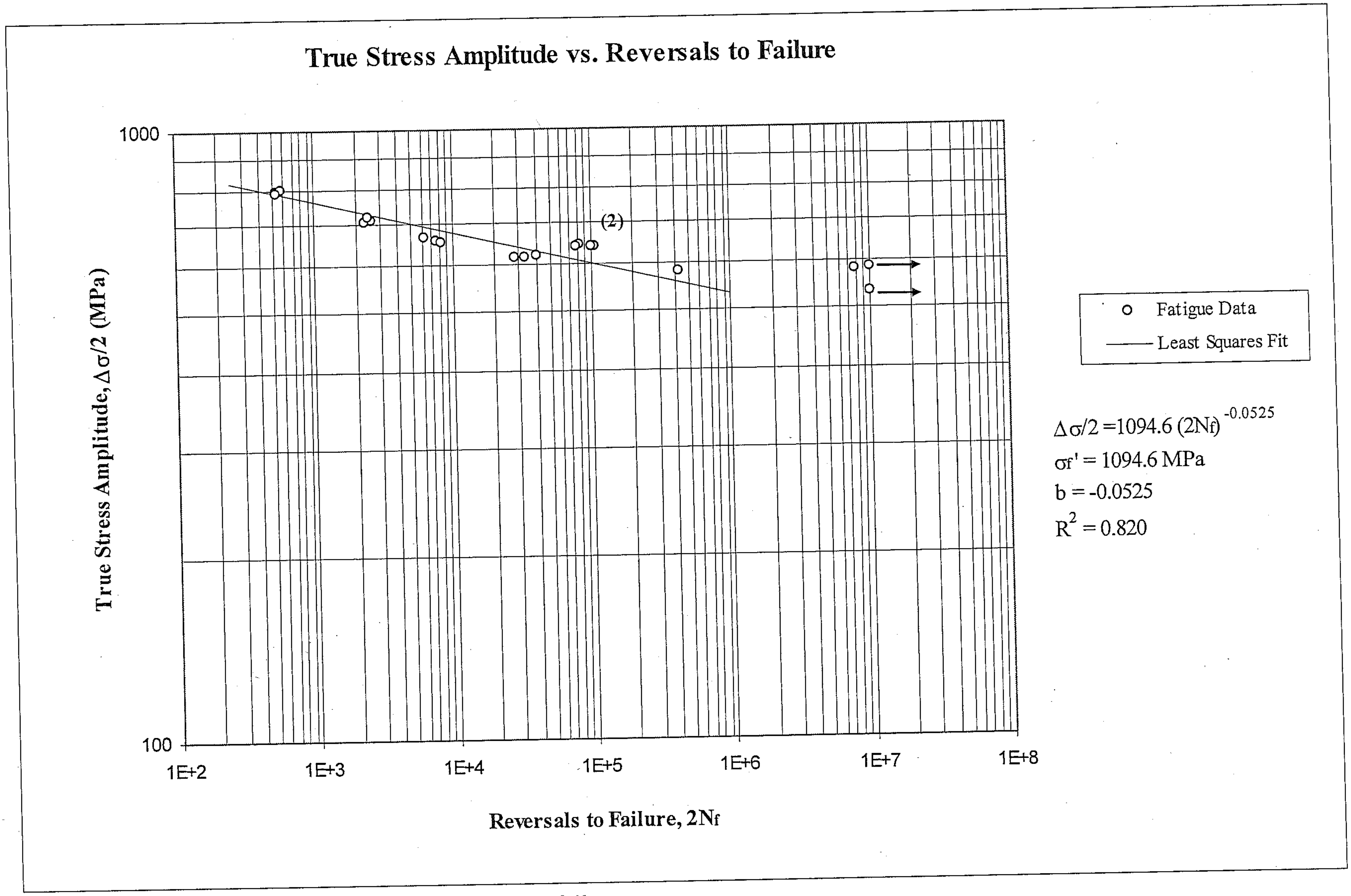

Figure 9: True stress amplitude versus reversals to failure

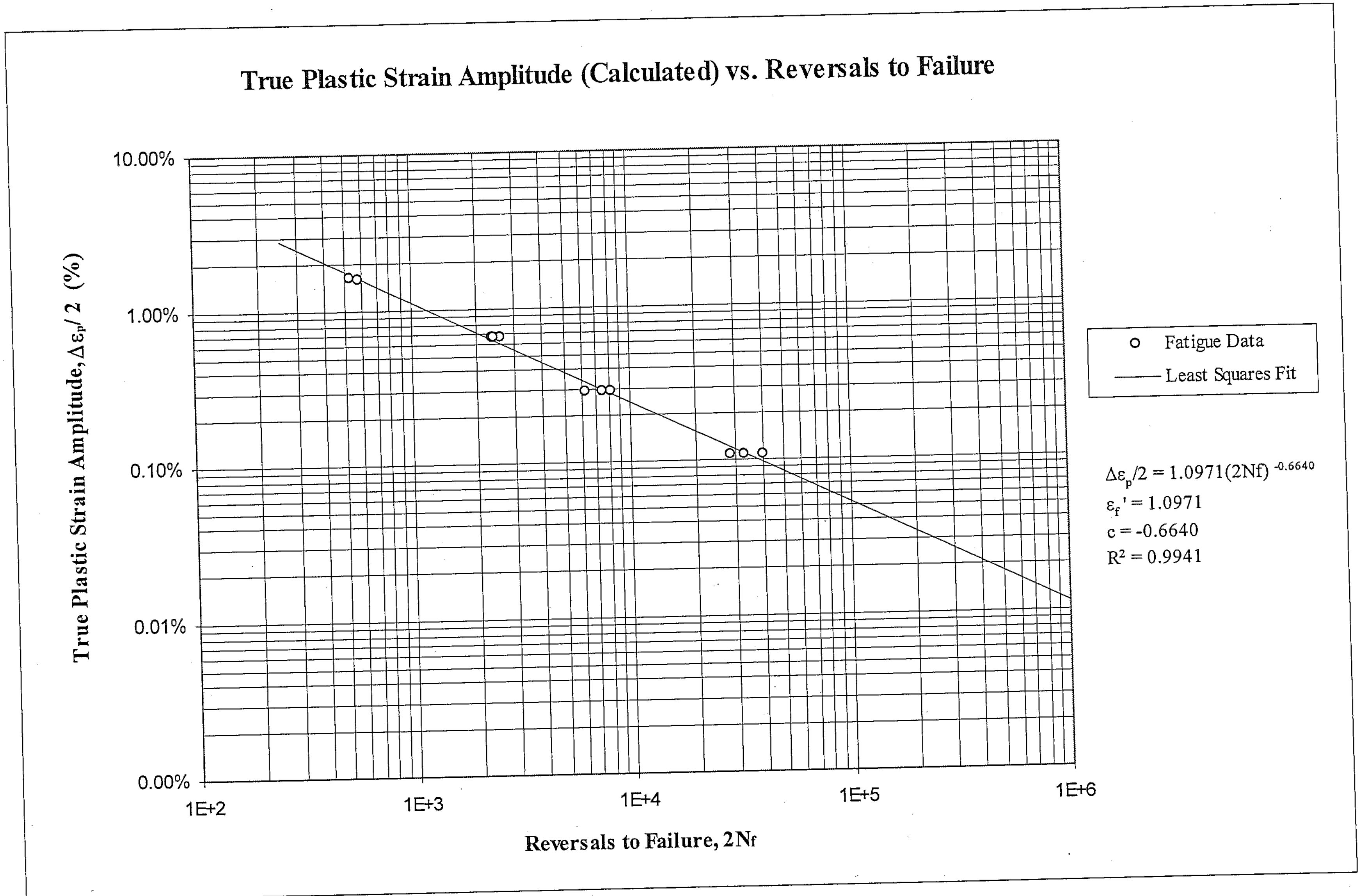

Figure 10: True plastic strain amplitude (calculated) versus reversals to failure

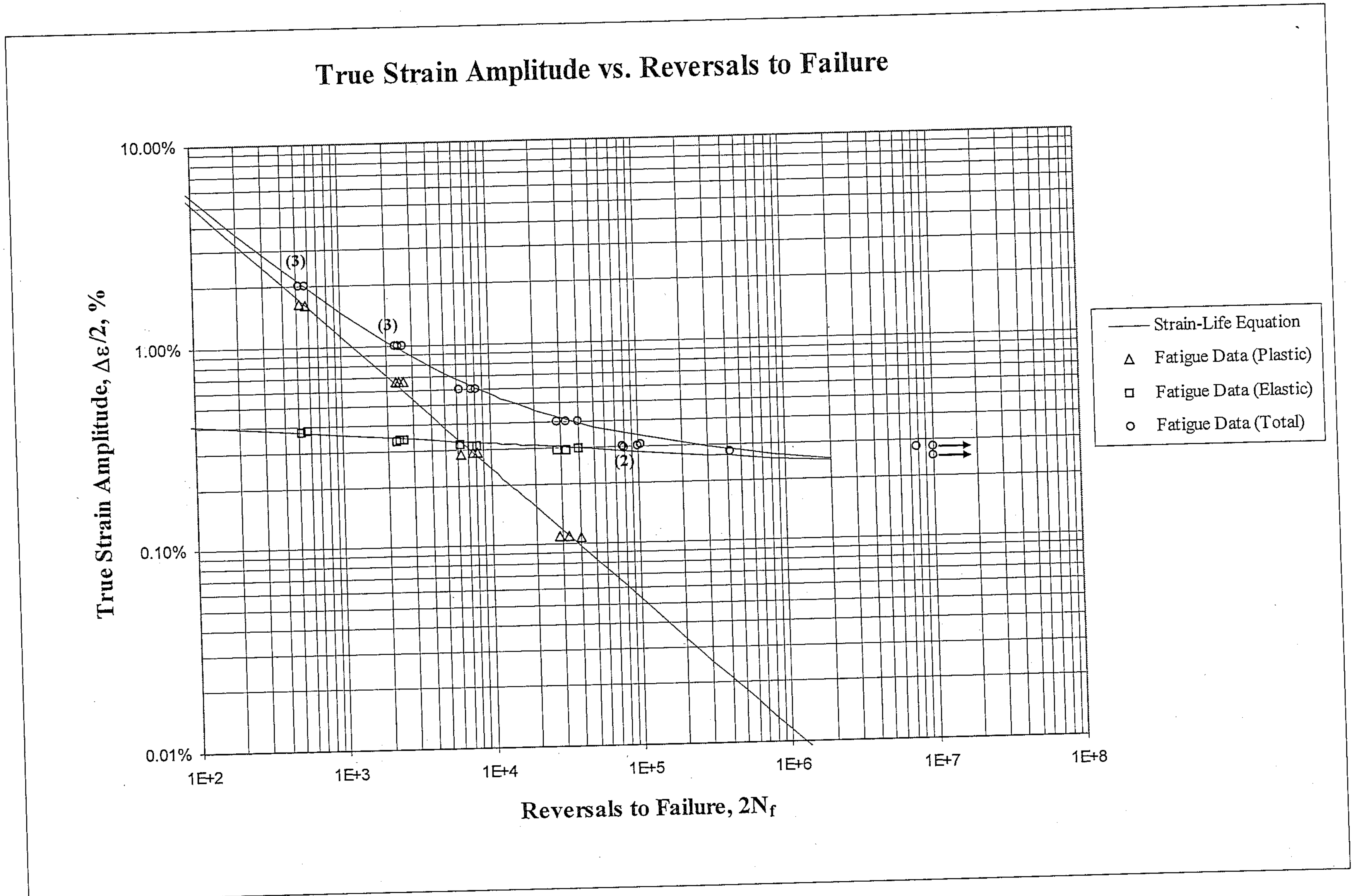

Figure 11: True strain amplitude versus reversals to failure

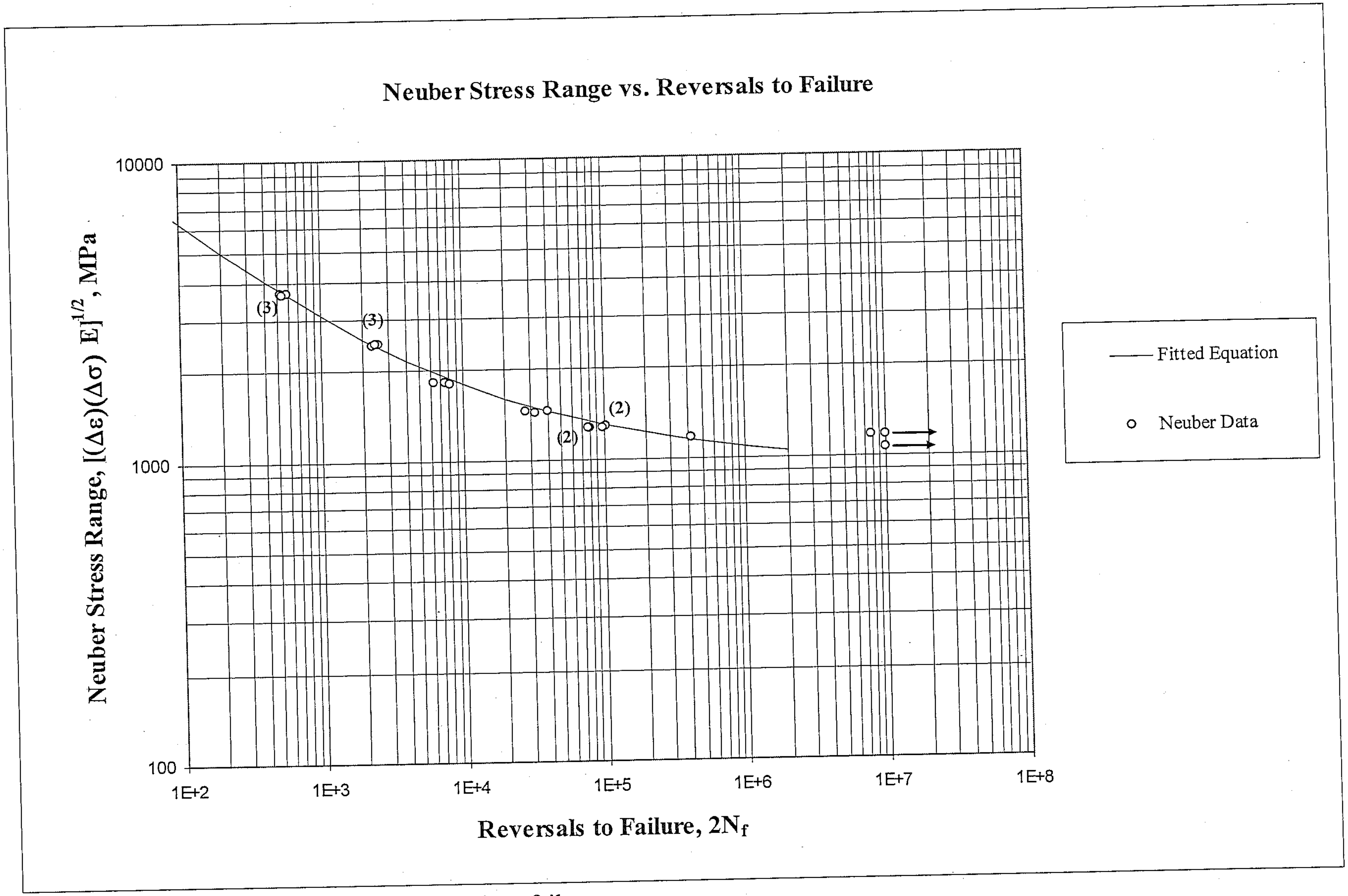

Figure 12: Neuber stress range versus reversals to failure

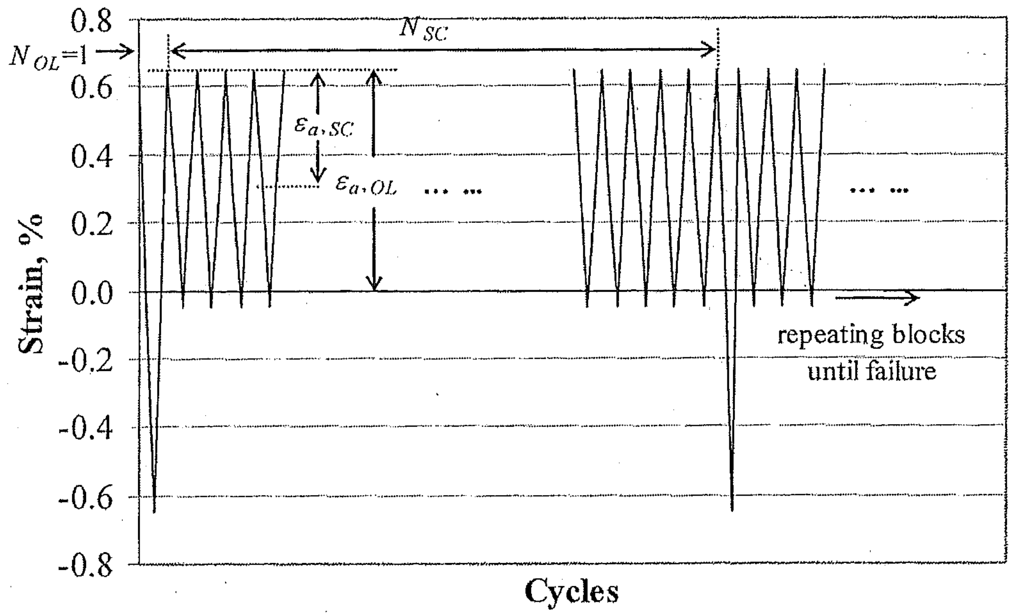

Figure 13: Periodic overload history

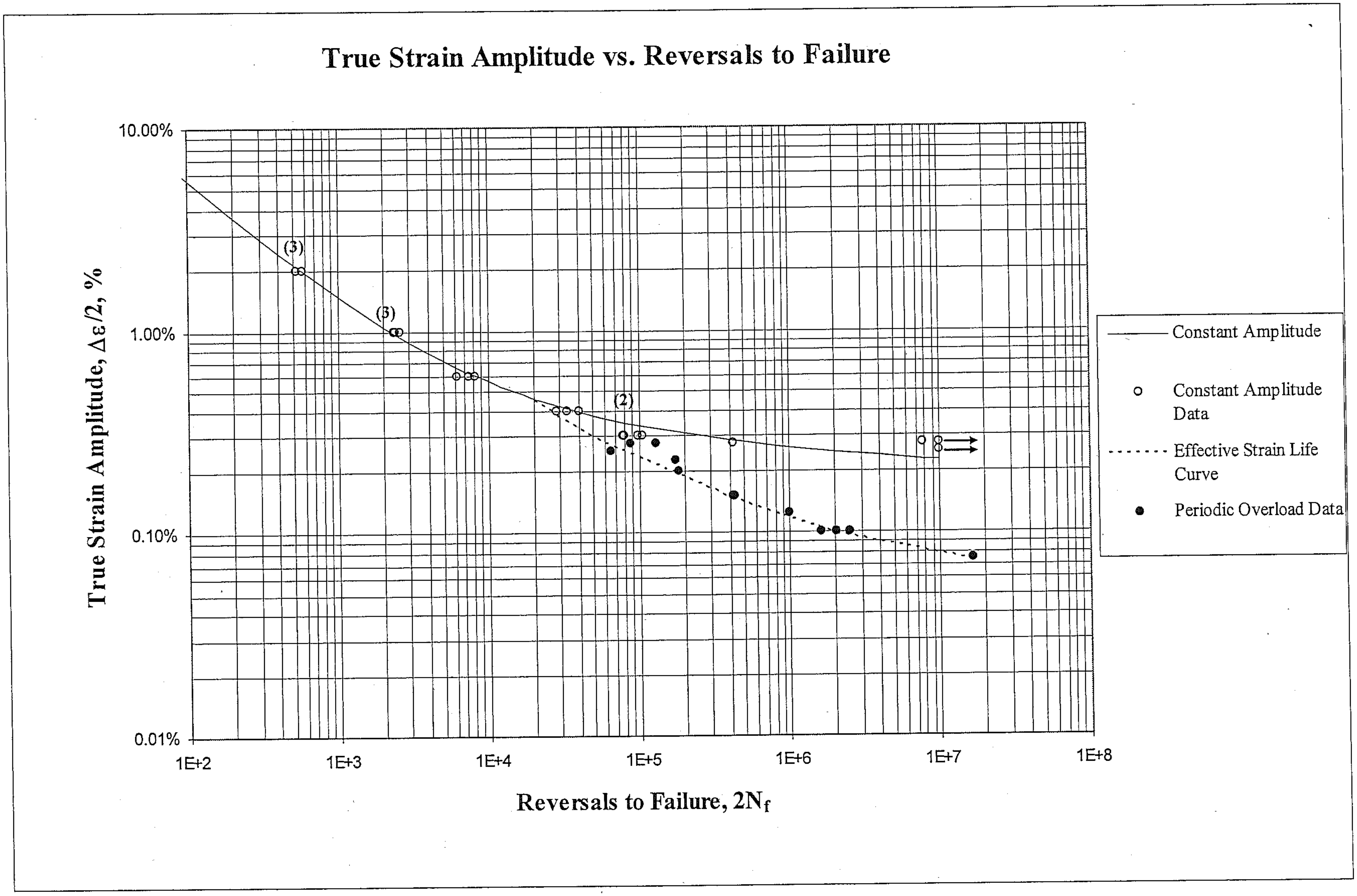

Figure 14: Periodic overload data superimposed with constant amplitude fatigue data

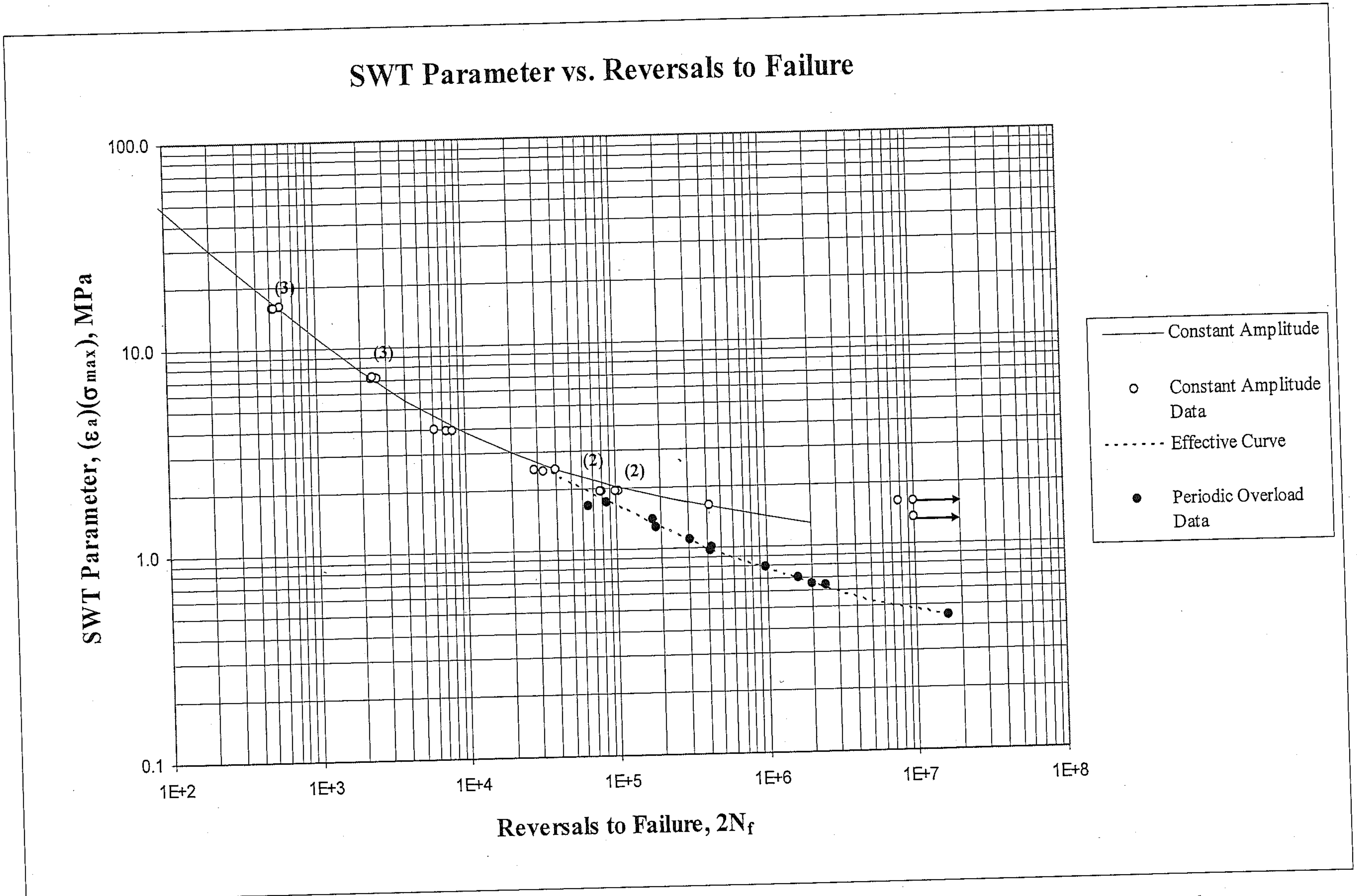

Figure 15: SWT parameter versus reversals to failure. Periodic overload data superimposed on constant amplitude data

REFERENCES

[1] ASTM Standard E606-92, "Standard Practice for Strain-Controlled Fatigue Testing," Annual Book of ASTM Standards, Vol. 03.01, 2004, pp. 593-606.

[2] ASTM Standard E83-02, "Standard Practice for Verification and Classification of Extensometers," Annual Book of ASTM Standards, Vol. 03.01, 2004, pp. 232-244.

[3] ASTM Standard E1012-99, "Standard Practice for Verification of Specimen Alignment Under Tensile Loading," Annual Book of ASTM Standards, Vol. 03.01, 2004, pp. 763-770.

[4] ASTM Standard E8-04, "Standard Test Methods for Tension Testing of Metallic Materials," Annual Book of ASTM Standards, Vol. 03.01, 2004, pp. 62-85.

[5] ASTM Standard E739-91, "Standard Practice for Statistical Analysis of Linear or Linearized Stress-Life (S-N) and Strain-Life (ε-N) Fatigue Data," Annual Book of ASTM Standards, Vol. 03.01, 1995, pp. 670-676.

[6] ASTM Standard E646-00, "Standard Test Method for Tensile Strain-Hardening Exponents (n-values) of Metallic Sheet Materials," Annual Book of ASTM Standards, Vol. 03.01, 2004, pp. 619-626.

[7] Stephens R. I., Fatemi A., Stephens R. R. and Fuchs H. O., "*Metal Fatigue in Engineering*", Second edition, Wiley Interscience, 2000.

Appendix A

Table A.1: Summary of monotonic tensile test results

Specimen ID	D_o, mm (in)	D_f, mm (in)	L_o, mm (in)	L_f, mm (in)	R, mm (in)	E, GPa (ksi)	YS (offset=0.2%), MPa (ksi)	UYS, MPa (ksi)	LYS, MPa (ksi)	YPE, %	S_u, MPa (ksi)	K, MPa (ksi)	n	%EL	%RA	ε_f, %	σ_f, MPa (ksi)
100_19	4.813 (0.1895)	2.769 (0.1090)	7.620 (0.3000)	10.45 (0.4115)	1.207 (0.0475)	211.6 (30,689)	882.8 (128.0)	897.26 (130.1)	882.8 (128.0)	0.0996%	943.6 (136.9)	1066.2 (154.6)	0.0235	37.2%	66.9%	110.6%	1312.8 (190.4)
100_16	4.788 (0.1885)	2.731 (0.1075)	7.620 (0.3000)	10.39 (0.4090)	1.207 (0.0475)	211.6 (30,689)	884.2 (128.2)	909.9 (132.0)	884.23 (128.2)	0.1507%	947.7 (137.4)	1080.7 (156.7)	0.0263	36.3%	67.5%	112.3%	1027.6 (149.0)
Average Values						211.6 (30,689)	883.5 (128.1)	903.58 (131.0)	883.515 (128.1)	0.1252%	945.7 (137.2)	1073.5 (155.7)	0.0249	36.8%	67.2%	111.5%	1170.2 (169.7)

Table A.2: Summary of constant amplitude completely reversed fatigue test results

Specimen ID	Test control mode	Test freq., Hz	E, GPa (ksi) [e]	At midlife ($N_{50\%}$) E', GPa (ksi)	$\Delta\varepsilon/2$, %	$\Delta\varepsilon_p/2$ (calculated), %	$\Delta\varepsilon_p/2$ (measured), %	$\Delta\sigma/2$, MPa (ksi)	σ_m, MPa (ksi)	$2N_{50\%}$, [a] reversals	$(2N_f)_{10\%}$, [b] reversals	$(2N_f)_{50\%}$, [c] reversals	Failure location [d]
100_03	strain	0.3	207.2 (30,045)	197.9 (28,705)	1.998%	1.623%	1.565%	793.0 (115.0)	-8.1 (-1.2)	256	-	524	IGL
100_07	strain	0.2	214.3 (31,082)	196.9 (28,557)	1.988%	1.609%	1.580%	800.1 (116.0)	-8.2 (-1.2)	256	-	580	IGL
100_06	strain	0.3	214.4 (31,091)	196.5 (28,492)	1.998%	1.625%	1.585%	787.2 (114.2)	-6.1 (-0.9)	256	522	530	IGL
100_02	strain	0.3	213.5 (30,970)	202.9 (29,420)	0.999%	0.662%	0.625%	712.0 (103.3)	-5.3 (-0.8)	1,024	2,580	2,598	IGL
100_04	strain	0.3	206.3 (29,913)	192.7 (27,941)	0.997%	0.663%	0.620%	705.8 (102.4)	-6.4 (-0.9)	1,024	2,322	2,344	IGL
100_10	strain	0.3	203.0 (29,434)	199.9 (28,985)	0.997%	0.660%	0.630%	717.6 (104.1)	-5.6 (-0.8)	1,024	2,400	2,418	IGL
100_01	strain	1.0	208.3 (3,021)	206.1 (2,990)	0.598%	0.289%	0.275%	654.4 (94.9)	-4.4 (-0.6)	4,096	7,502	7,536	IGL
100_11	strain	1.0	210.4 (30,516)	200.0 (29,007)	0.599%	0.285%	0.263%	663.9 (96.3)	-3.4 (-0.5)	2,048	6,038	6,244	IGL
100_14	strain	1.0	208.3 (30,234)	196.7 (28,543)	0.596%	0.289%	0.265%	650.4 (94.3)	-3.2 (-0.5)	4,096	8,000	8,216	IGL
100_09	strain	5.0	212.4 (30,799)	205.9 (29,886)	0.399%	0.109%	0.103%	613.1 (88.9)	-9.2 (-1.3)	16,384	32,006	33,094	IGL
100_13	strain	5.0	208.0 (30,162)	196.6 (28,529)	0.400%	0.108%	0.095%	618.7 (89.7)	-15.0 (-2.2)	16,384	38,358	40,130	IGL
100_20	strain	5.0	210.8 (30,566)	202.3 (29,364)	0.400%	0.109%	0.095%	615.3 (89.2)	2.6 (0.4)	16,384	27,120	28,364	IGL
100_18	strain load	1.0 10.0	214.5 (31,109)	214.3 (31,102)	0.304%	0.000%	0.000%	640.8 (92.9)	0.0 (0.0)	65,536	-	104,976	IGL
100_22	strain load	1.0 10.0	212.3 (30,789)	212.8 (30,888)	0.296%	0.000%	0.000%	643.3 (93.3)	0.0 (0.0)	32,768	-	80,962	IGL
100_23	strain load	1.0 10.0	208.8 (30,287)	214.0 (31,062)	0.300%	0.000%	0.000%	640.8 (92.9)	0.0 (0.0)	32,768	-	78,074	IGL
100_21	load	10.0	-	-	0.300%	0.000%	0.000%	640.8 (92.9)	0.0 (0.0)	32,768	-	99,388	IGL
100_05	load	25.0	-	-	0.275%	0.000%	0.000%	578.8 (83.9)	0.0 (0.0)	131,072	-	419,144	IGL
100_08	load	24.0	-	-	0.275%	0.000%	0.000%	580.8 (84.2)	0.0 (0.0)	4,194,304	-	7,763,276	IGL
100_15	load	25.0	-	-	0.275%	0.000%	0.000%	581.9 (84.4)	0.0 (0.0)	-	-	>10,000,000	No Failure
100_24	load	24.0	213.1 (30,900)	214.3 (31,105)	0.250%	0.000%	0.000%	532.6 (77.2)	0.0 (0.0)	-	-	>10,000,000	No Failure

[a] $2N_{50\%}$ is defined as the midlife reversal ; [b] $2(N_f)_{10\%}$ is defined as reversal of 10% load drop

[c] $2(N_f)_{50\%}$ is defined as reversal of 50% load drop or failure

[d] IGL = Inside gage length;

[e] E value was calculated from the first cycle

Table A.3: Summary of the periodic overload fatigue test results

Spec. ID	Test Control Mode	Test Freq. OL/SC (Hz)	E (GPa) [b]	Load history Description: ε_a, SC (%)	ε_m, SC (%)	$\Delta\varepsilon_p/2$, SC (calculated) (%)	σ_a, SC (MPa)	σ_m, SC (MPa)	N_{SC} (Cycles)	ε_a, OL (%)	$\Delta\varepsilon_p/2$, OL (calculated) (%)	σ_a, OL (MPa)	σ_m, OL (MPa)	$N_{f, OL}$ (Cycles)	Exp. Life (Blks)	$N_{f, sc(eq)}$ (Cycles)	OL Damage Ratio	Failure Location [a]
104_02	Strain	1 / 4	204.7	0.275%	0.183%	0.024%	513.2	104.6	100	0.458%	0.129%	671.6	-60.2	10,090	419	43,715	0.042	IGL
104_04	Strain	1 / 4	200.6	0.250%	0.206%	0.014%	473.1	177.9	100	0.456%	0.112%	689.0	-50.8	10,090	315	32,515	0.031	IGL
104_05	Strain	1 / 4	200.3	0.225%	0.231%	0.008%	434.1	176.8	100	0.456%	0.132%	648.8	-49.5	10,090	812	88,307	0.080	IGL
104_06	Strain	1 / 4	201.5	0.200%	0.260%	0.006%	389.7	239.7	100	0.460%	0.124%	675.3	-22.8	10,090	841	91,747	0.083	KE
104_14	Strain	1 / 7	199.8	0.175%	0.285%	0.003%	343.4	285.0	100	0.459%	0.122%	674.2	-26.1	10,090	1,351	155,986	0.134	IGL
104_07	Strain	1 / 7	199.9	0.150%	0.309%	0.004%	292.2	356.3	300	0.459%	0.110%	699.3	-33.0	10,090	660	211,858	0.065	KE
104_11	Strain	1 / 7	201.6	0.150%	0.310%	0.004%	294.4	375.5	300	0.459%	0.110%	704.0	-19.8	10,090	669	214,952	0.066	IGL
104_08	Strain	1 / 7	201.0	0.125%	0.335%	0.003%	245.4	383.2	300	0.460%	0.128%	667.7	-17.2	10,090	1,419	495,365	0.141	IGL
104_09	Strain/Load	1 / 7	201.2	0.100%	0.360%	0.003%	195.0	497.3	1,000	0.460%	0.116%	692.6	0.1	10,090	745	804,393	0.074	KE
104_10	Strain	1 / 7	199.6	0.100%	0.360%	0.002%	195.9	453.2	1,000	0.460%	0.112%	695.3	-21.4	10,090	914	1,005,041	0.091	KE
104_13	Strain	1 / 7	206.2	0.100%	0.360%	0.002%	201.2	433.0	1,000	0.460%	0.130%	680.0	-22.0	10,090	1,108	1,244,680	0.110	IGL
104_12	Strain/Load	1 / 7	192.7	0.075%	0.386%	0.001%	142.2	454.4	1,000	0.460%	0.134%	629.2	-12.0	10,090	4,525	8,204,358	0.448	KE

[a] IGL = Inside gage length, KE = At knife edge
[b] E value was calculated from the first cycle
All stress values reported are from midlife

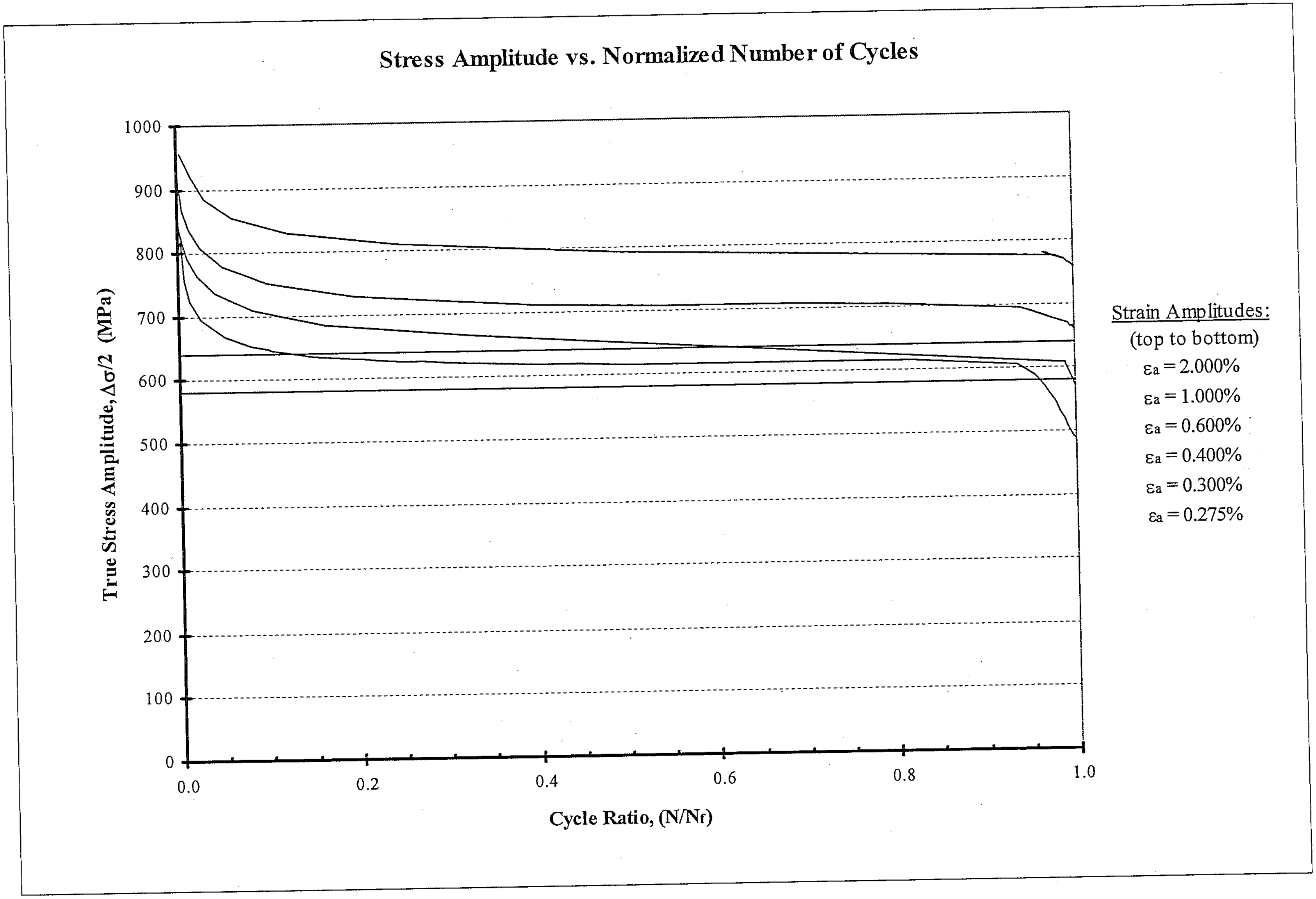

Figure A.1a: True stress amplitude versus normalized number of cycles

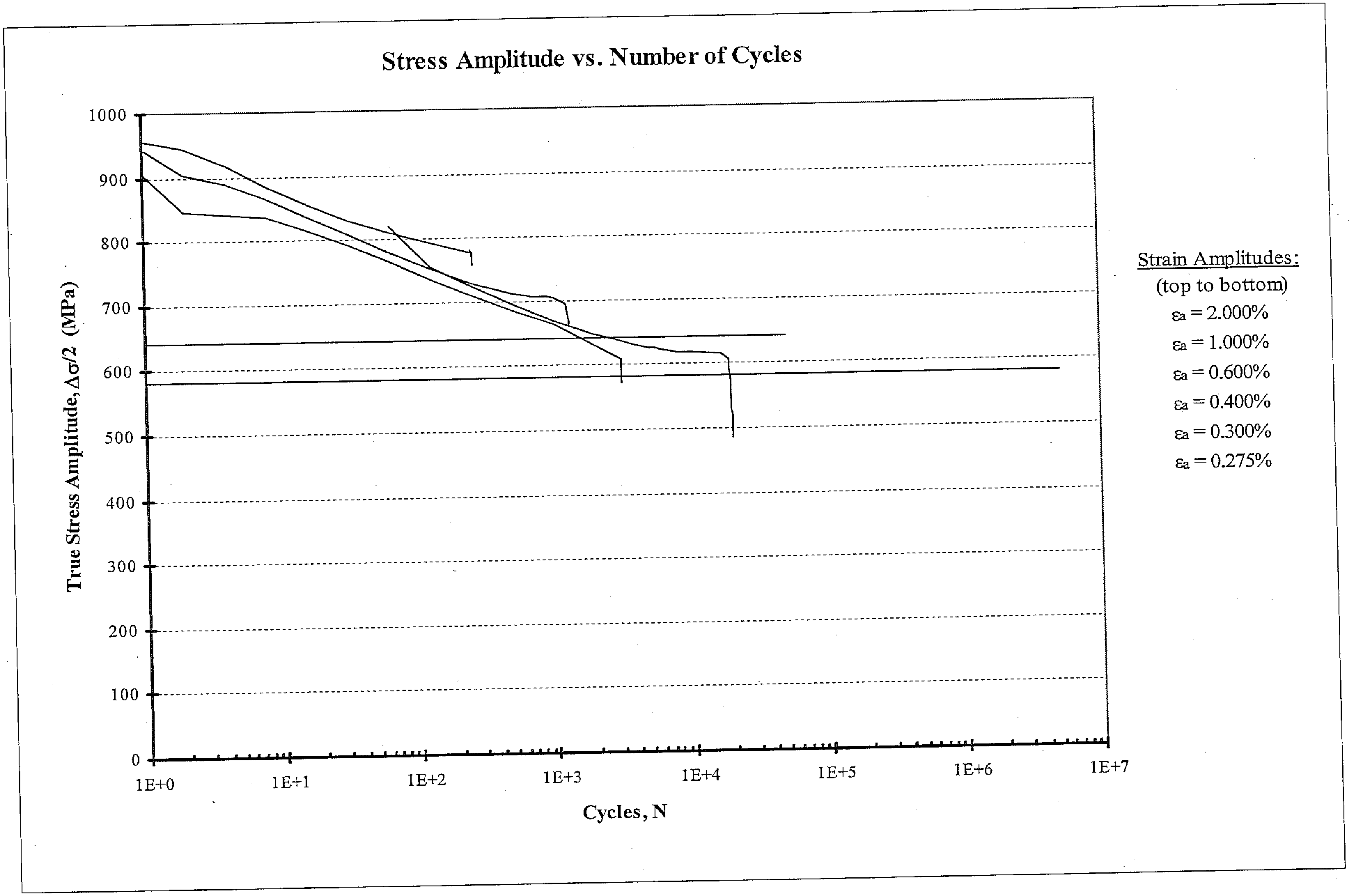

Figure A.1b: True stress amplitude versus number of cycles

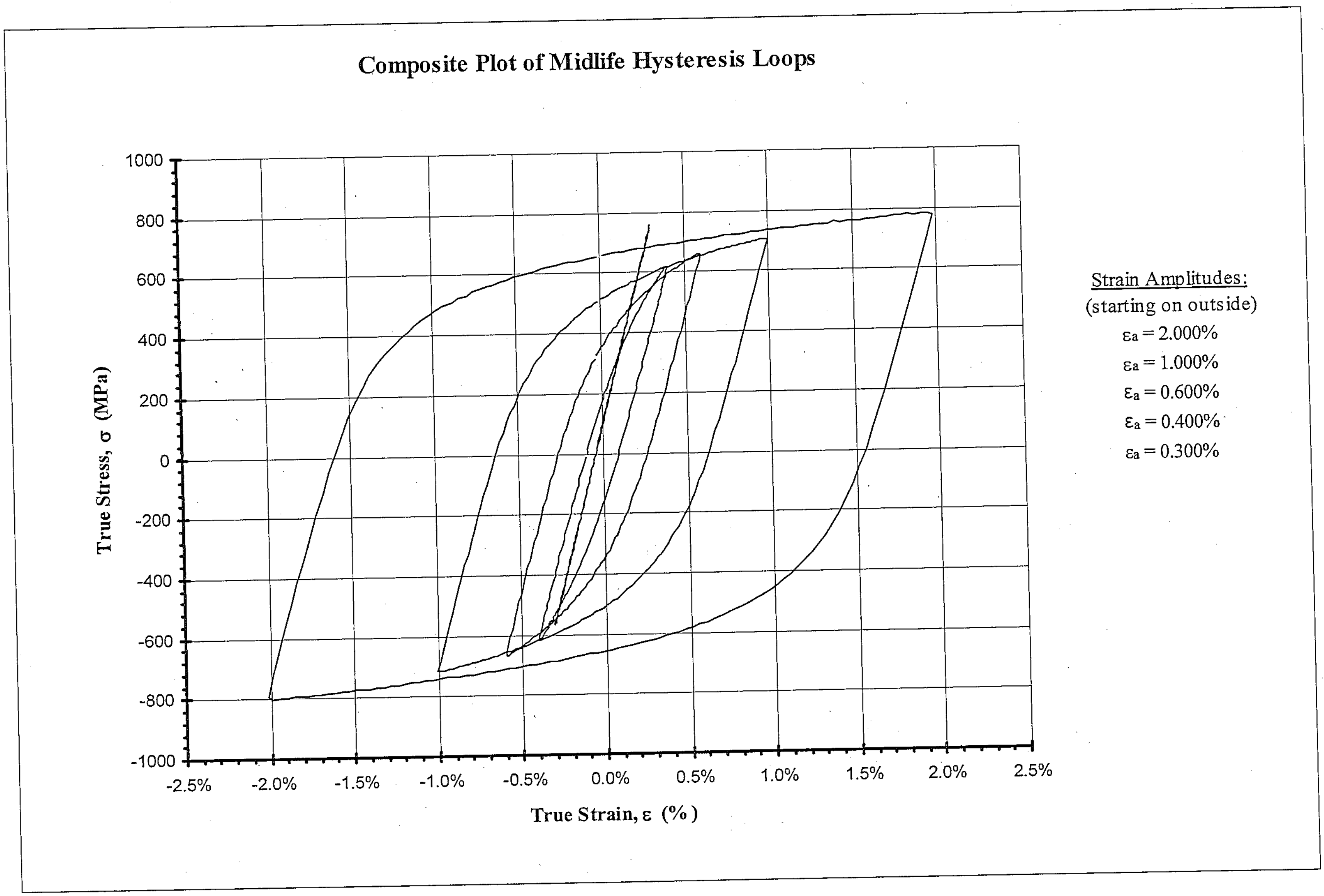

Figure A.2: Composite plot of midlife hysteresis loops

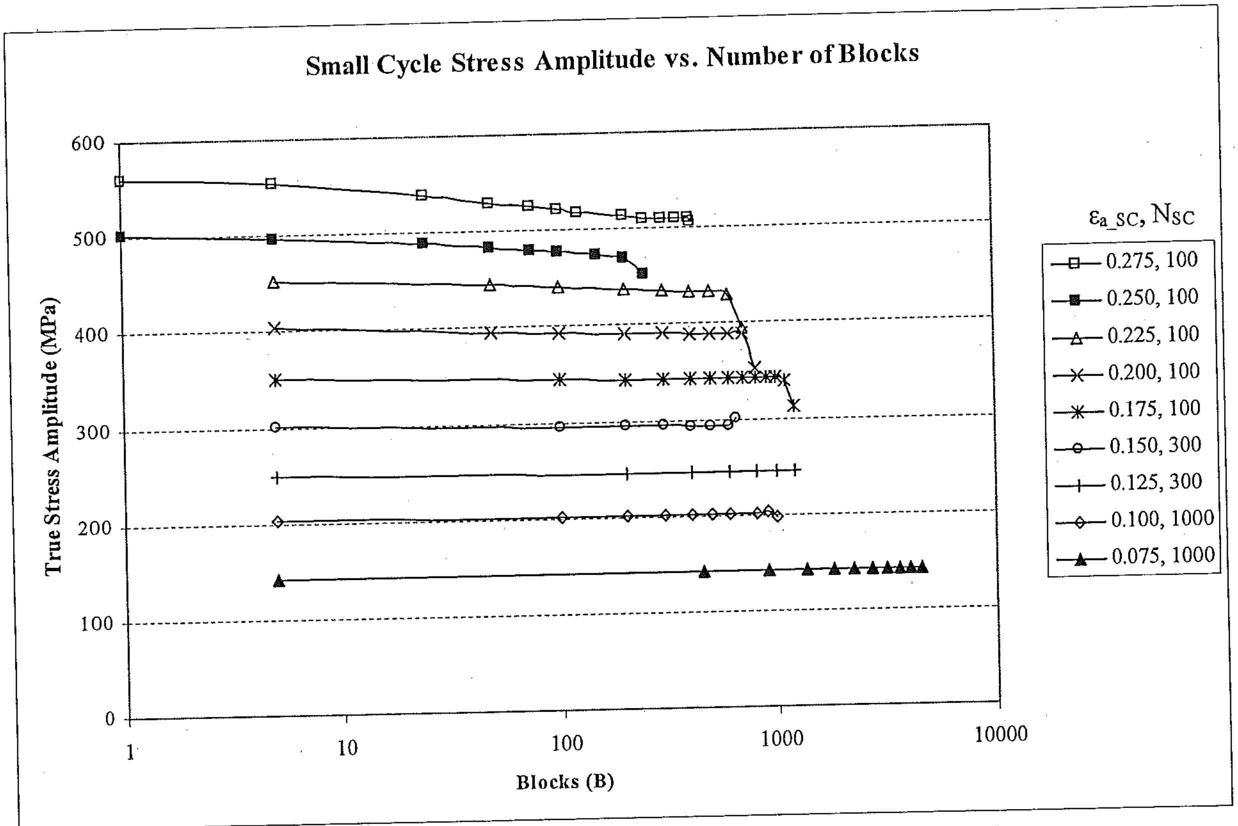

Figure A.3a: Small cycle amplitude transient response throughout the life.

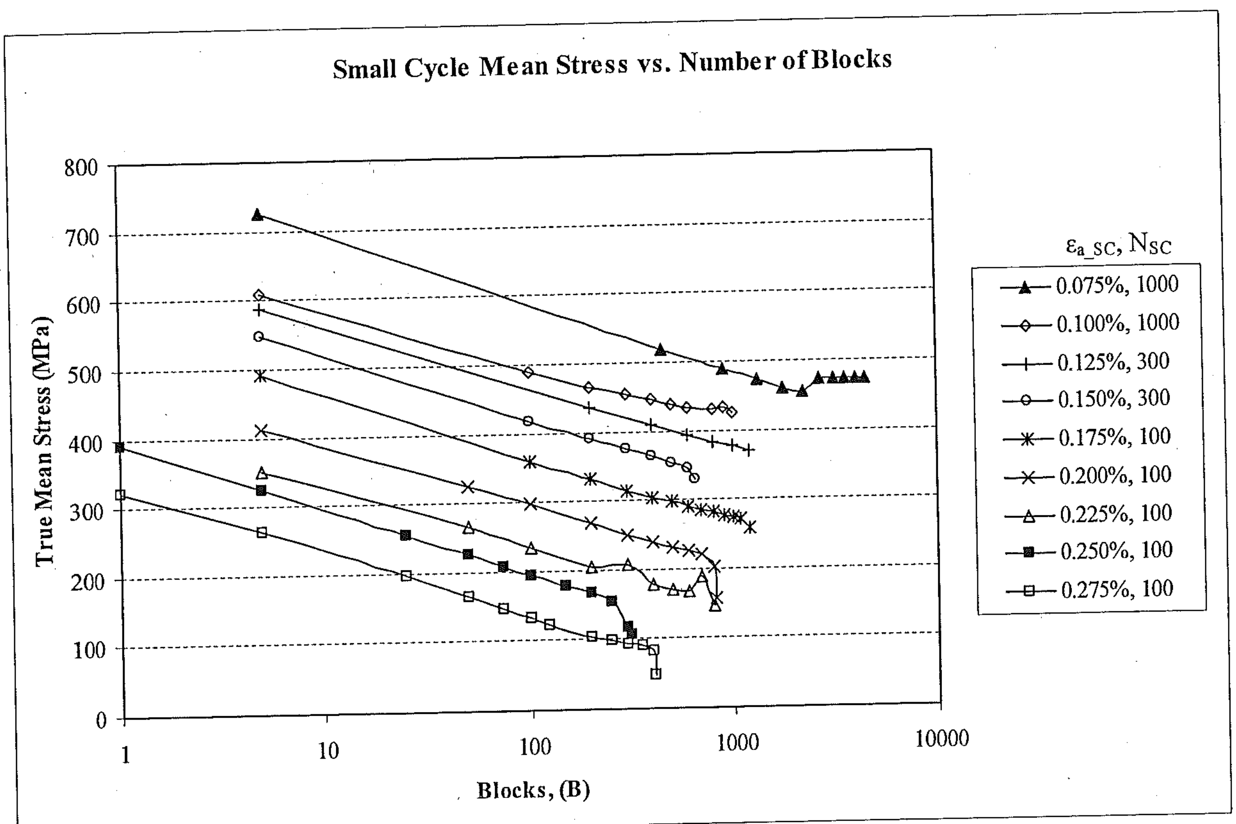

Figure A.3b: Small cycle mean transient response throughout the life.

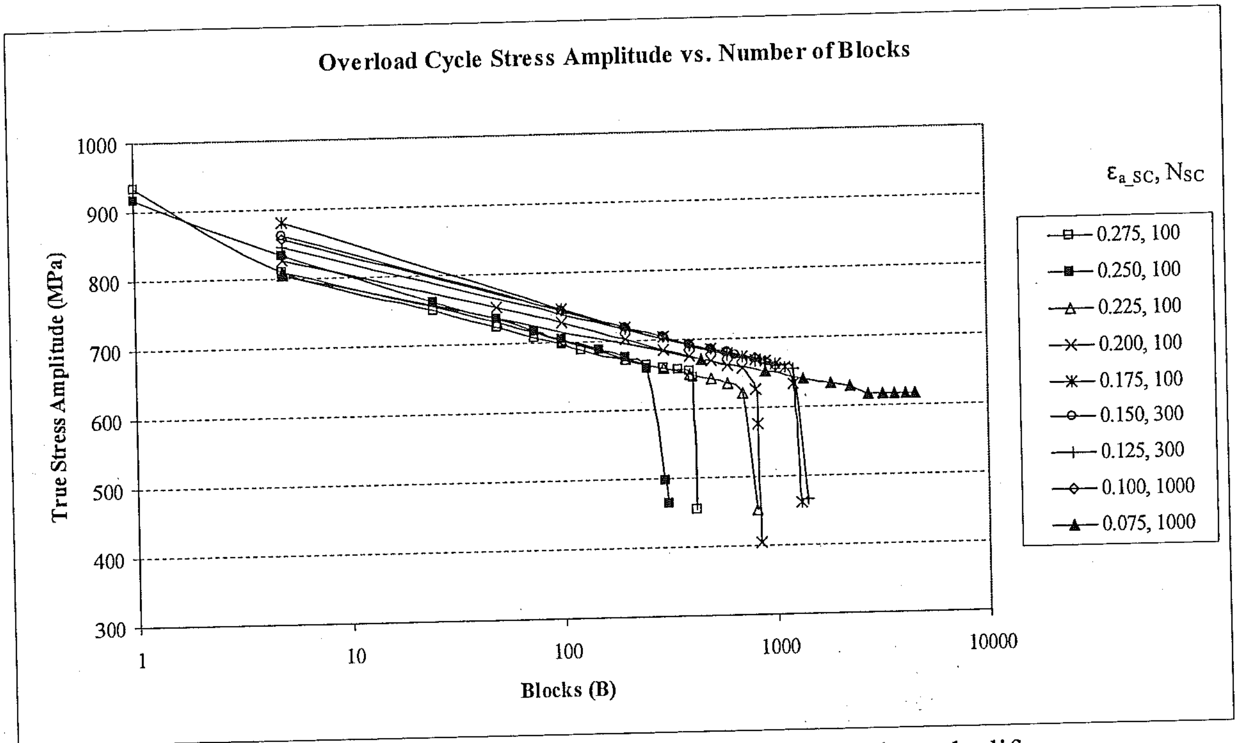

Figure A.4a: Overload cycle amplitude transient response throughout the life.

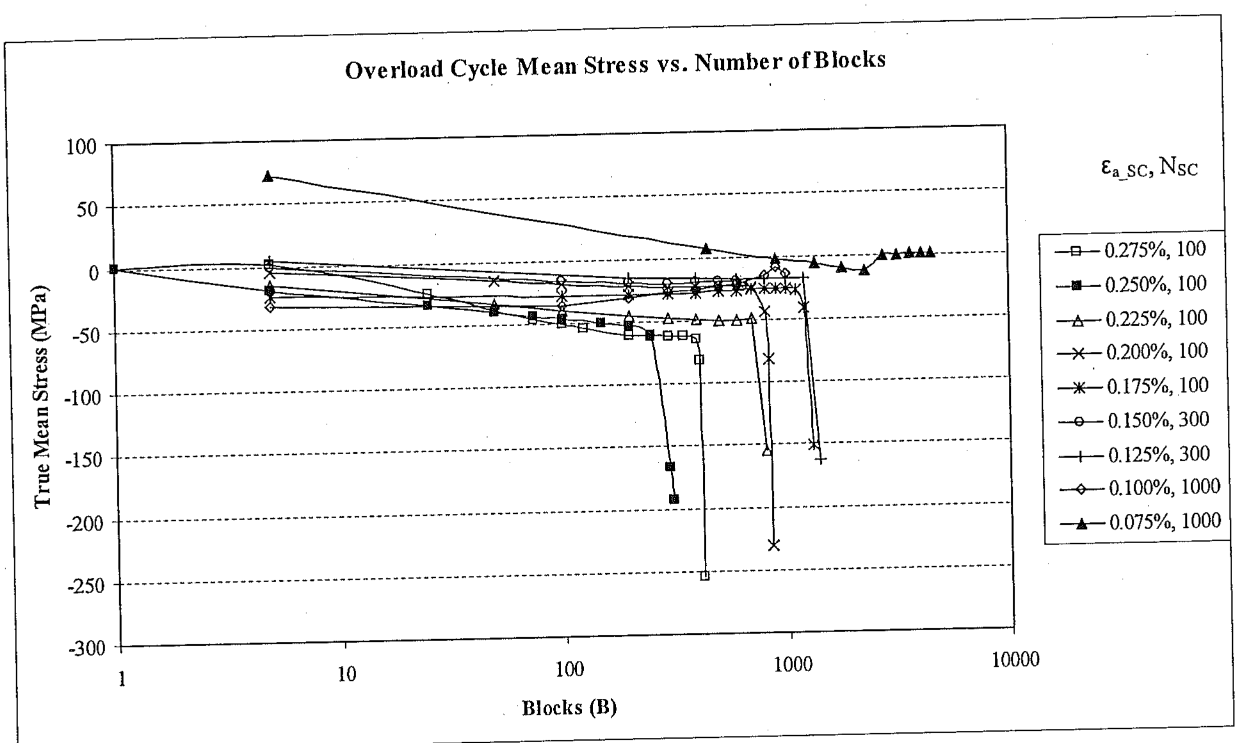

Figure A.4b: Overload cycle mean transient response throughout the life.

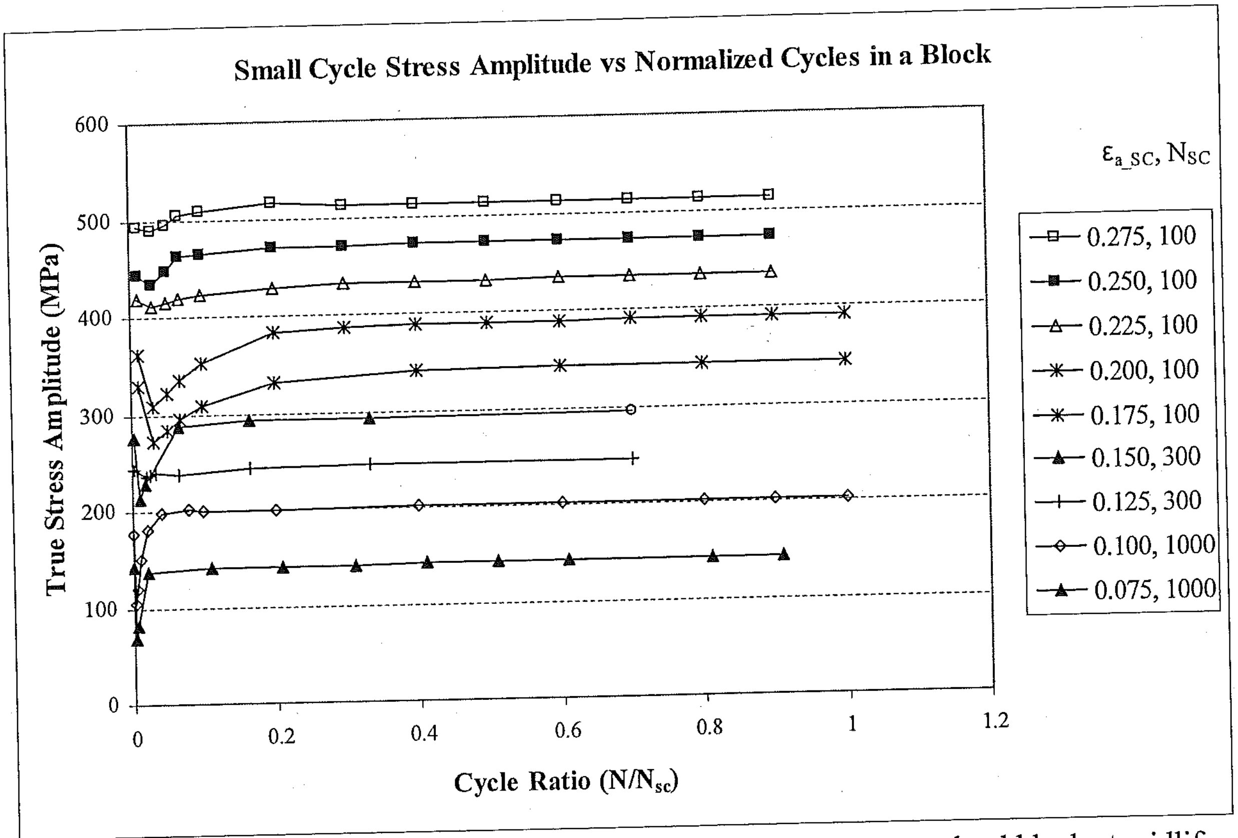

Figure A.5a: Small cycle transient response amplitude throughout one load block at midlife.

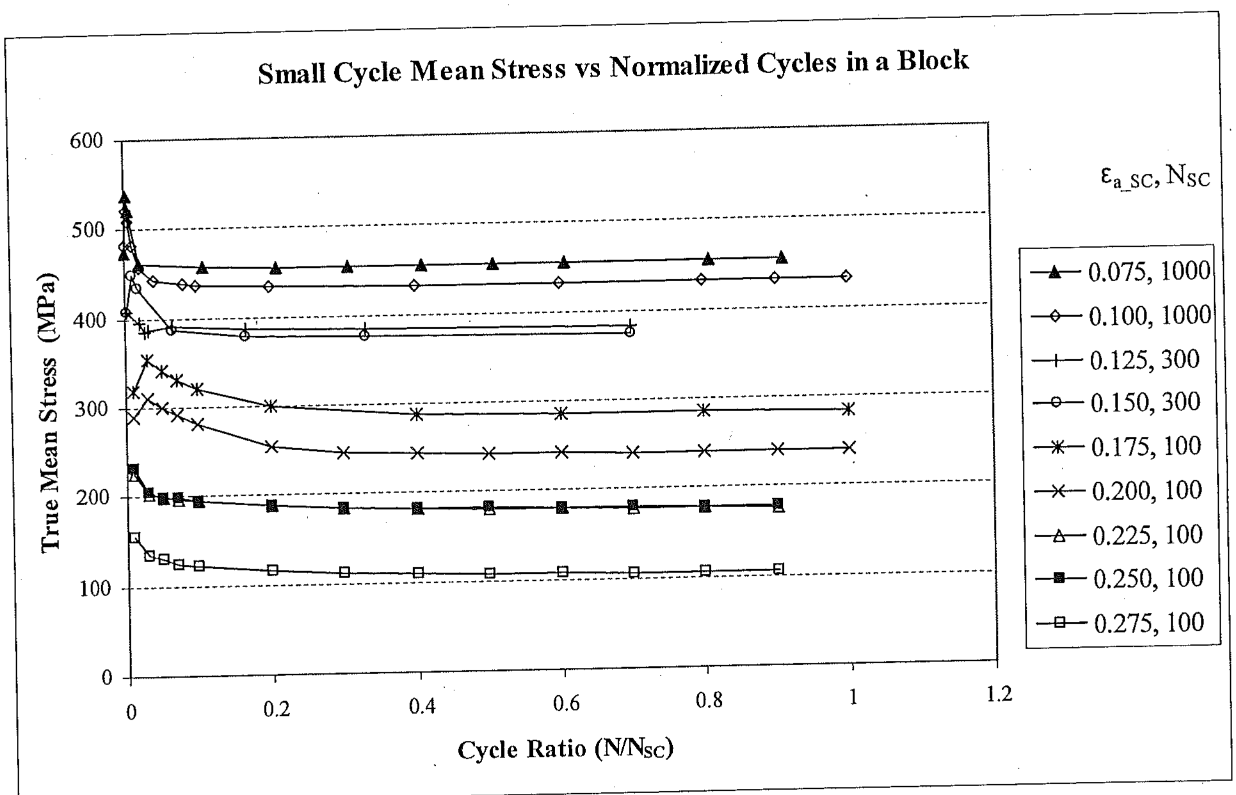

Figure A.5b: Small cycle transient response mean throughout one load block at midlife.

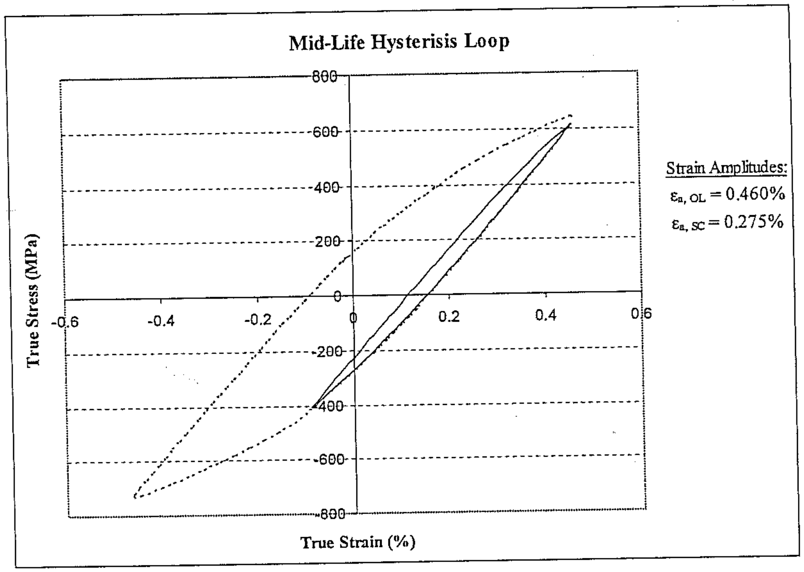

(a)

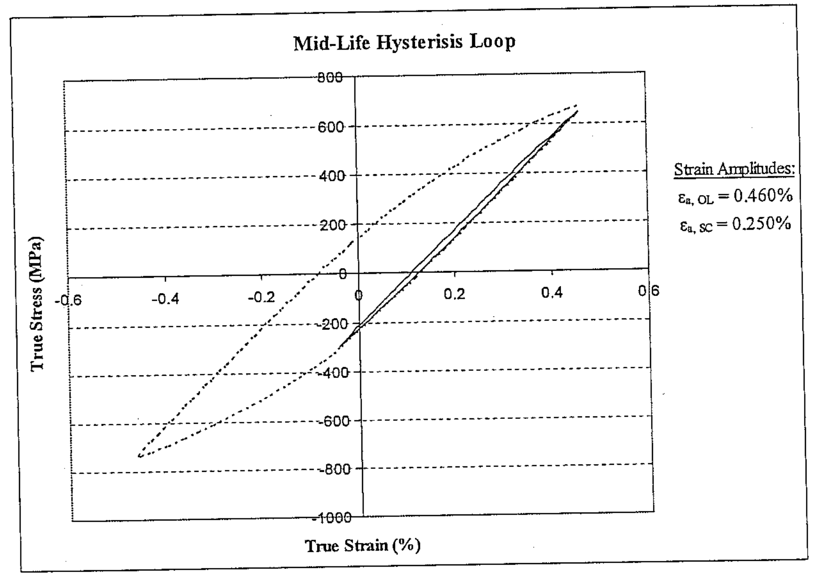

(b)

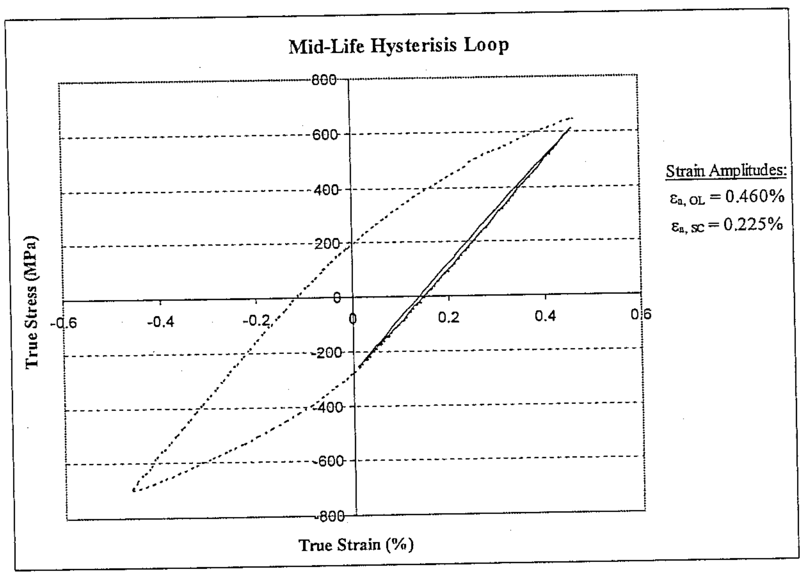

(c)

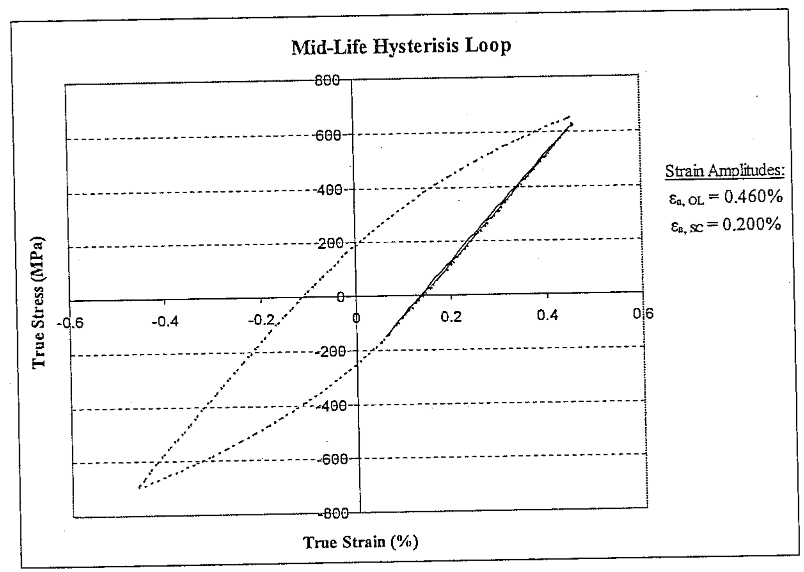

(d)

Figure A.6(a-i): Periodic overload midlife hysterisis loop superimposed with small cycle midlife hysterisis loop

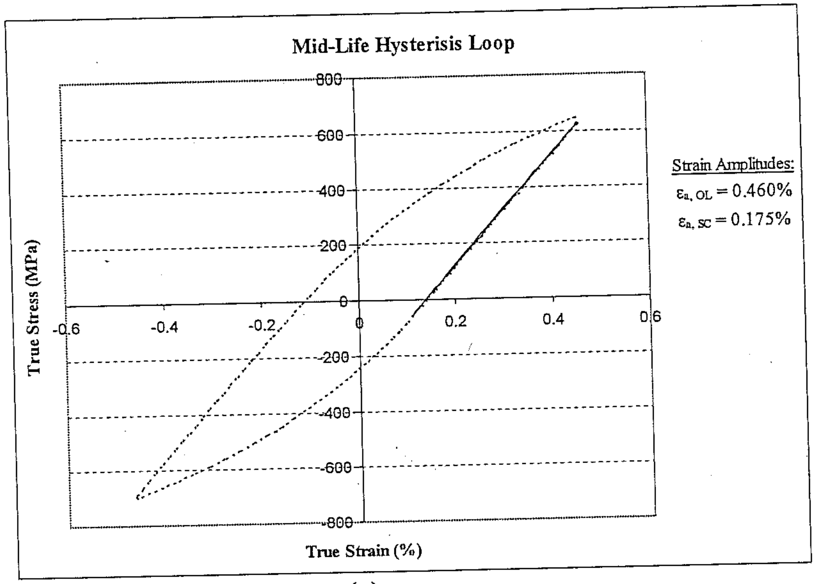

(e)

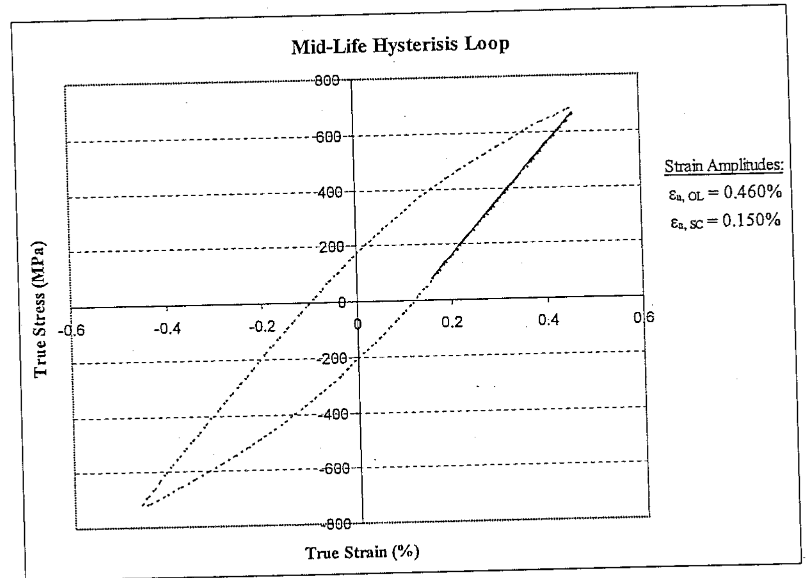

(f

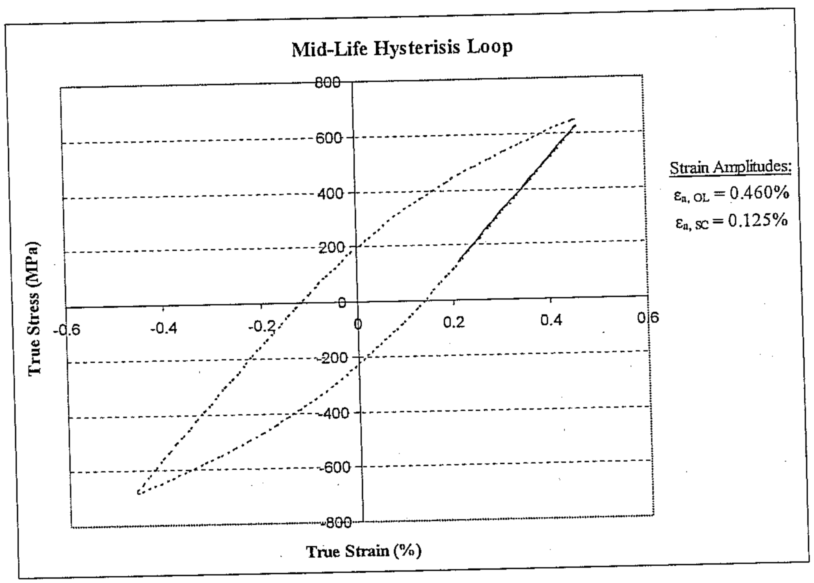

(g)

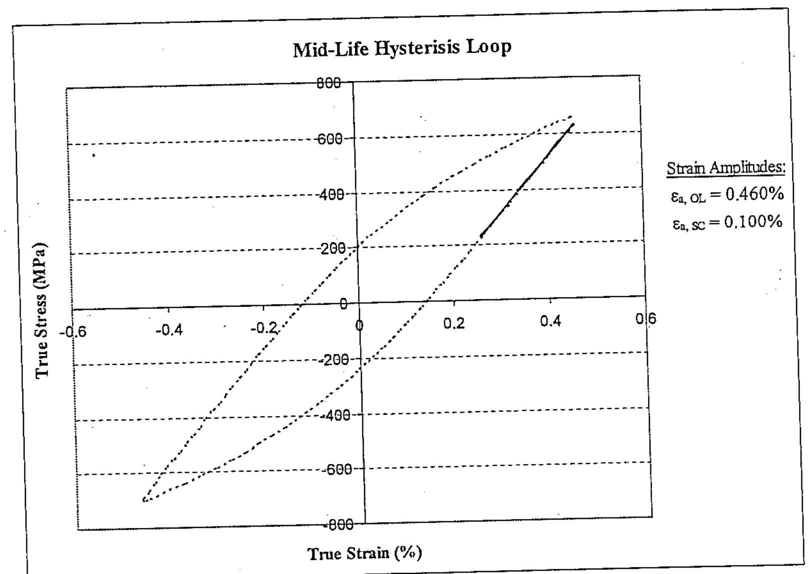

(h)

Figure A.6(a-i): Periodic overload midlife hysterisis loop superimposed with small cycle midlife hysterisis loop

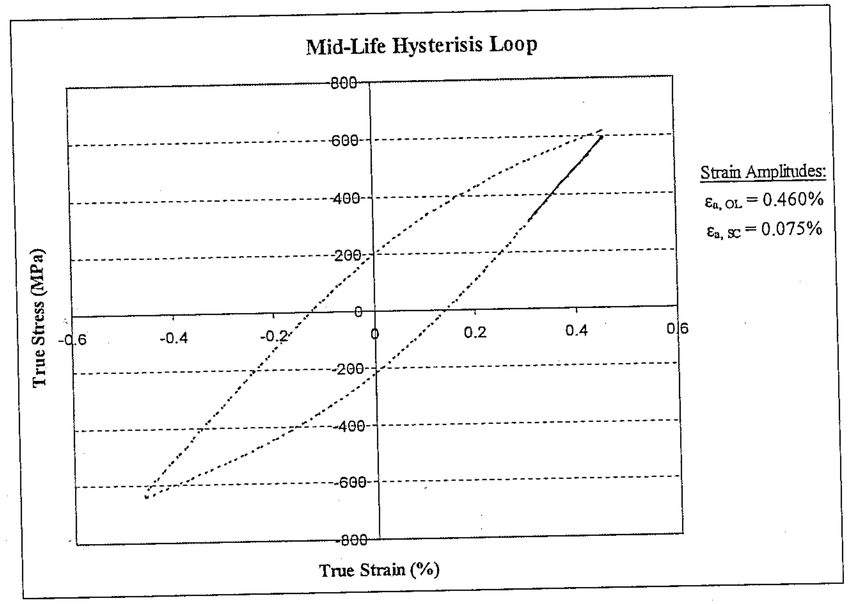

(i)

Figure A.6(a-i): Periodic overload midlife hysterisis loop superimposed with small cycle midlife hysterisis loop

Appendix B

UAW - Chrysler

SCIENTIFIC LABS & PROVING GROUNDS

CHRYSLER

Materials Engineering Lab Report

LTR Number: 130899

To: Peter Bauerle **Phone:** 776-7387

Location: CTC

From: Mechanical Properties **Completed:** 11/20/2007

Metallography

Subject/Part Name: Fatigue Specimen-Iteration 100/104
Report Status: Complete
Originator: Peter Bauerle
Originator Phone: 248-576-7387
Number of Parts: 1
Nature of Work: Process/Materials Development
Vendor:
Plant:
P/N:
MS:
PS:

History of Part

The sample that has been submitted is a fatigue specimen that will be used for the development of the AISI fatigue database, iterations 100 & 104. The test speciman was prepared from an 8822 steel grade with low side chemistry. The sample has been quench and tempered by austenitizing at 1700F prior to quenching in 150F oil and then tempering at 1050F to an aim hardness of 25-30 HRC.

Test Results

Mechanical Properties – 130899

Hardness - Rockwell (Performed By: Greg Cornelissen)

Grip end (surface hardness) - 32.0 HRC 32.0 HRC 31.5 HRC

Hardness - Micro (Performed By: Greg Cornelissen)

Newage Microhardness Tester - 1000gf

Microhardness traverse across the gage section starting from the edge staggered in increments of .005" up to a depth of .030" followed by .010" increments beyond this point to the core.

.005"	35.8 HRC
.010"	32.8 HRC
.015"	32.0 HRC
.020"	32.5 HRC
.025"	33.3 HRC
.030"	32.0 HRC
.040"	31.6 HRC
.050"	30.1 HRC
.060"	30.2 HRC
.070"	29.6 HRC
.080"	29.4 HRC
.090"	30.4 HRC
.100"	29.6 HRC

Metallography - 130899

General Microstructure Description (Performed By: Jin Dong)

A fatigue Specimen-Iteration 100/104 was sectioned longitudinally from the grip end and transversely from the gage section to conduct a general microstructure description.

The sample was prepared with standard test procedures for sectioning, mounting, polishing, and etched with 3% nital. The sample was reviewed and microphotographs were taken using an Olympus PMG3 Microscope.

The microphotographs revealed that the entire sample consisted of tempered martensite. There is some evidence of banding in the longitudinal section from the grip end.

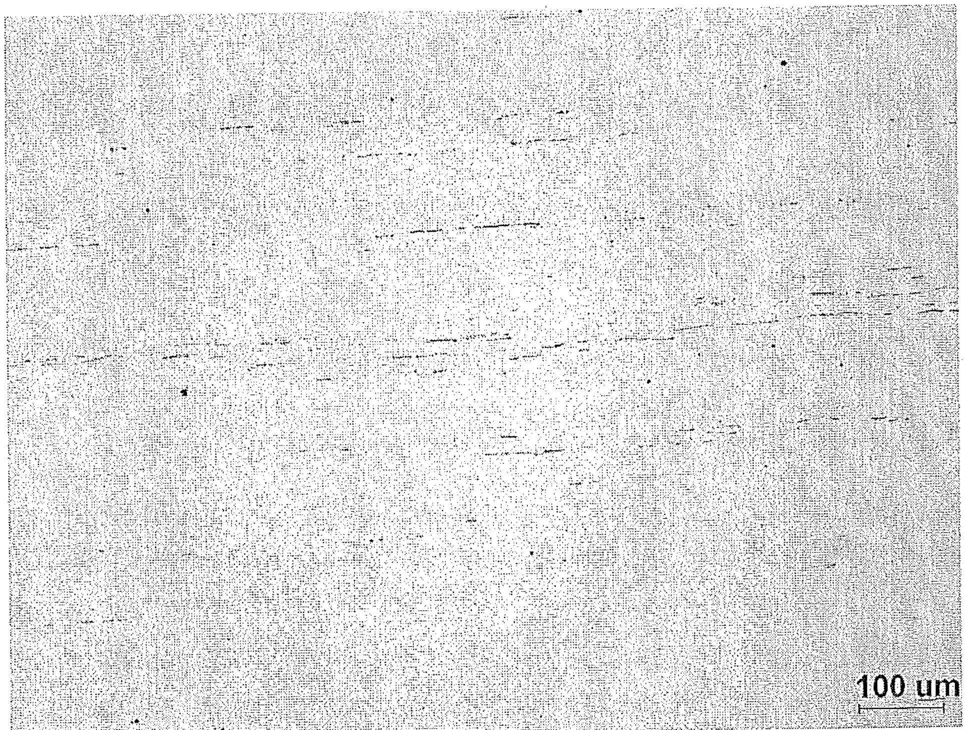

Fig. 1 View of the inclusion distribution in the steel.

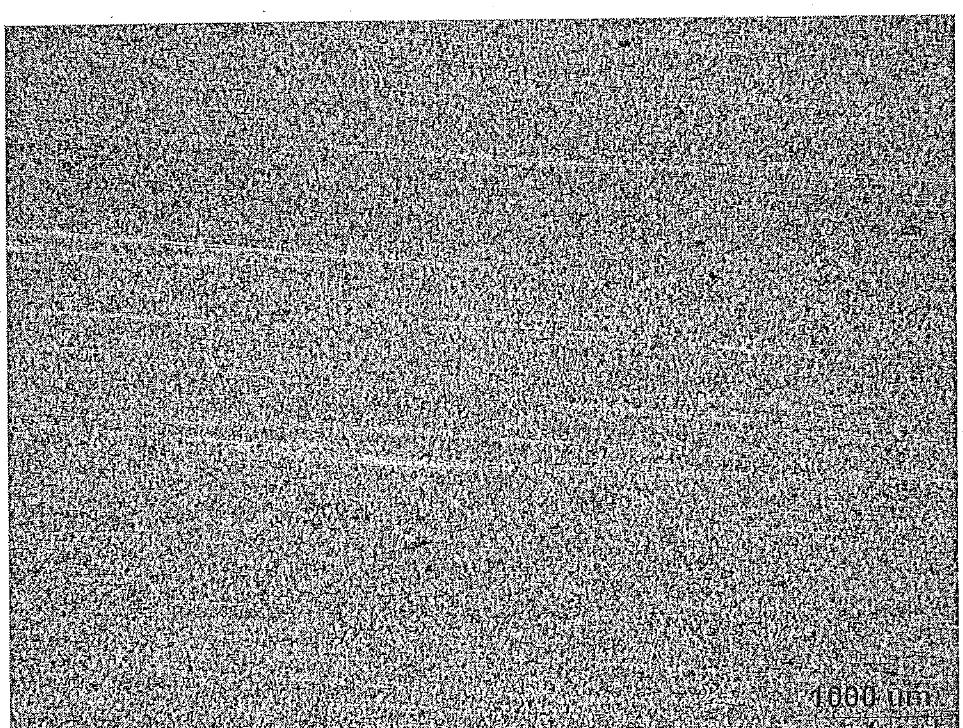

Fig. 2 Overall view of the longitudinal section from the grip end.

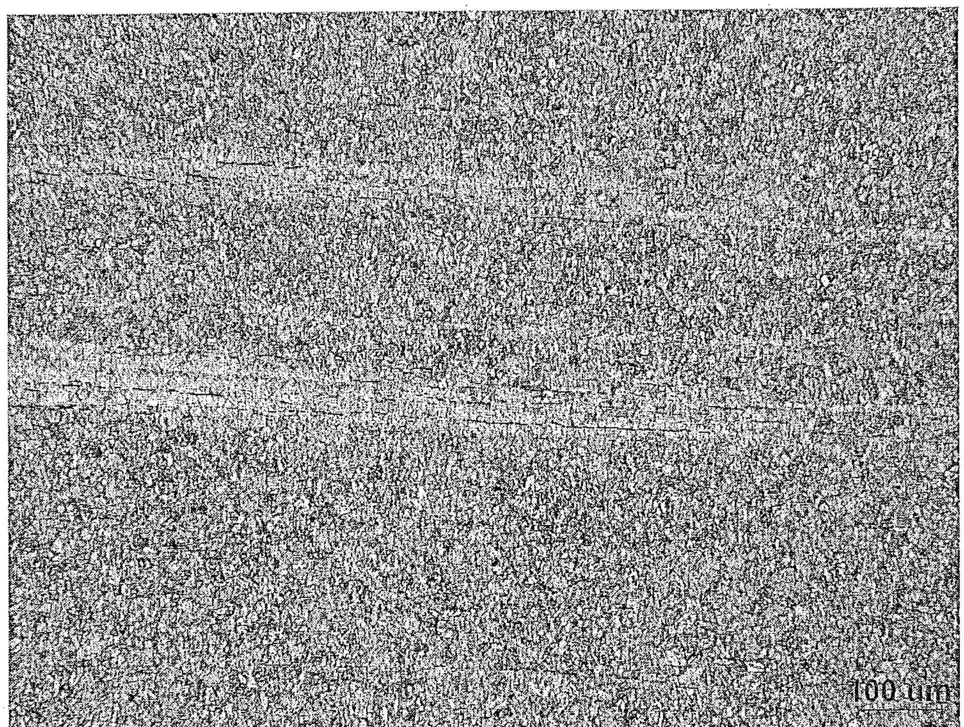

Fig. 3 Low magnification showing the microstructure in the longitudinal section of the grip end.

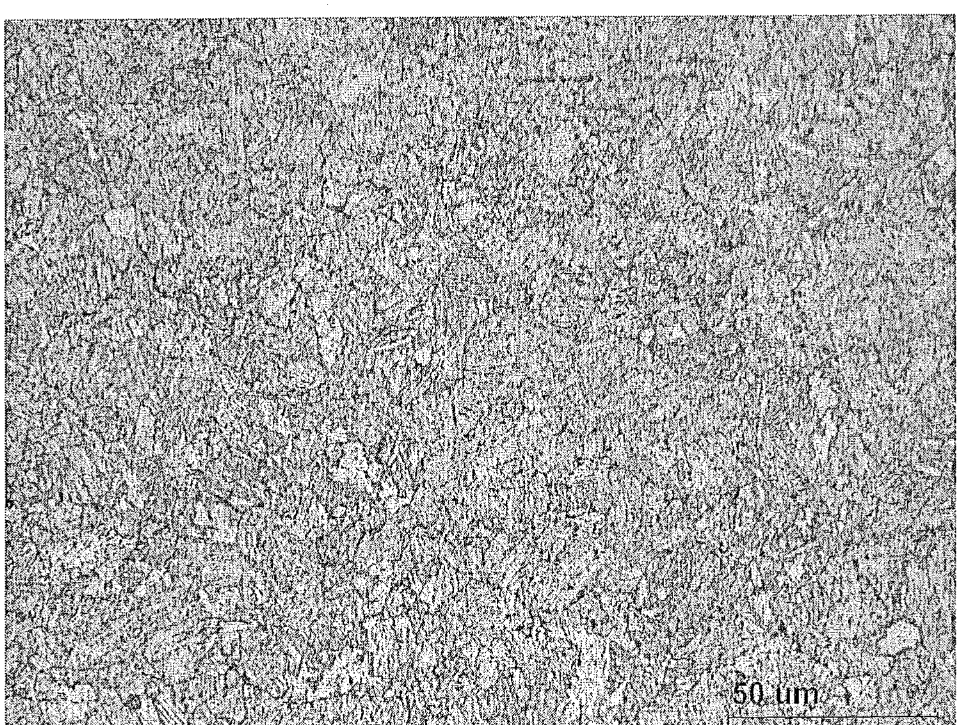

Fig. 4 High magnification showing the microstructure in the longitudinal section from the grip end.

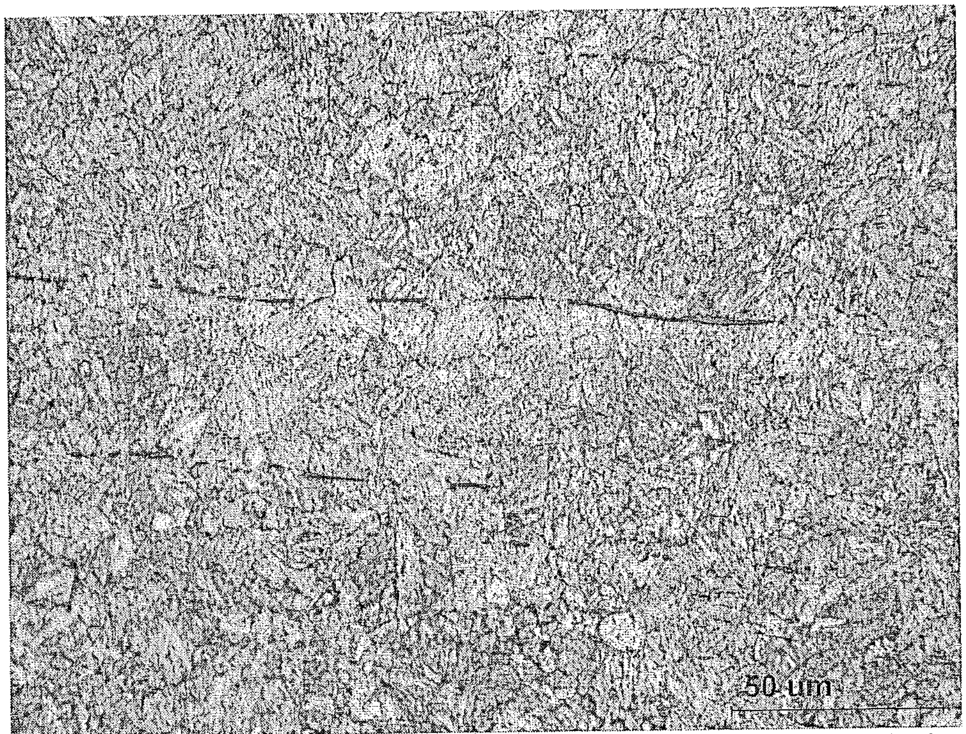

Fig. 5 High magnification showing the microstructure in the longitudinal section from the grip end

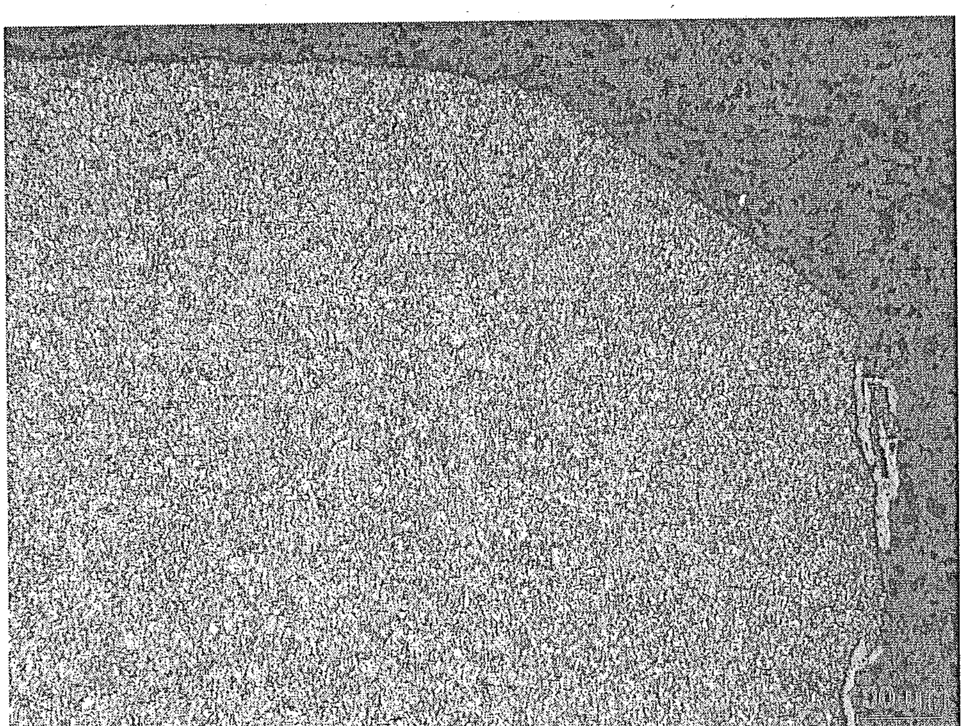

Fig. 6 Low magnification showing the microstructure in the longitudinal section (surface area) from the grip end.

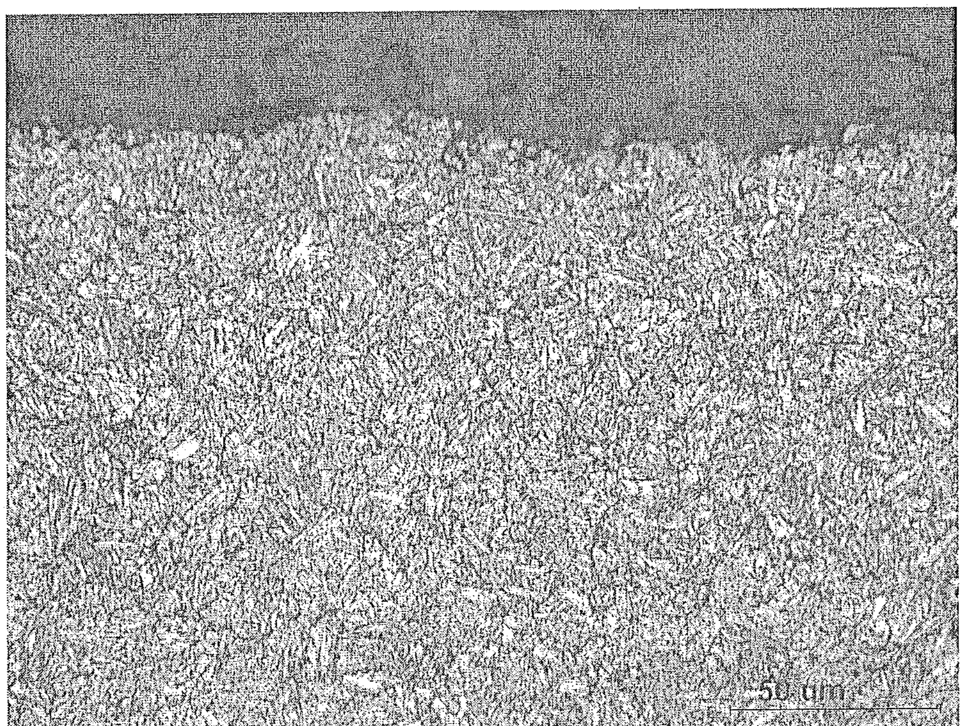

Fig. 7 High magnification showing the microstructure in the longitudinal section (surface area) from the grip end.

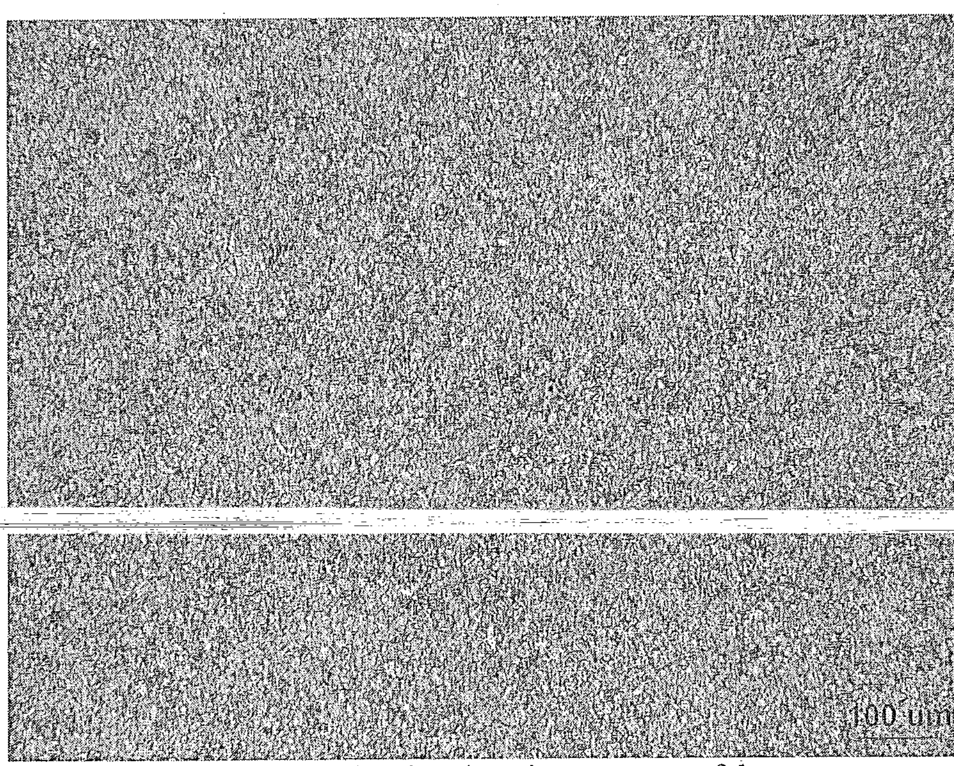

Fig. 8 Low magnification showing the microstructure of the transverse section from the gage area.

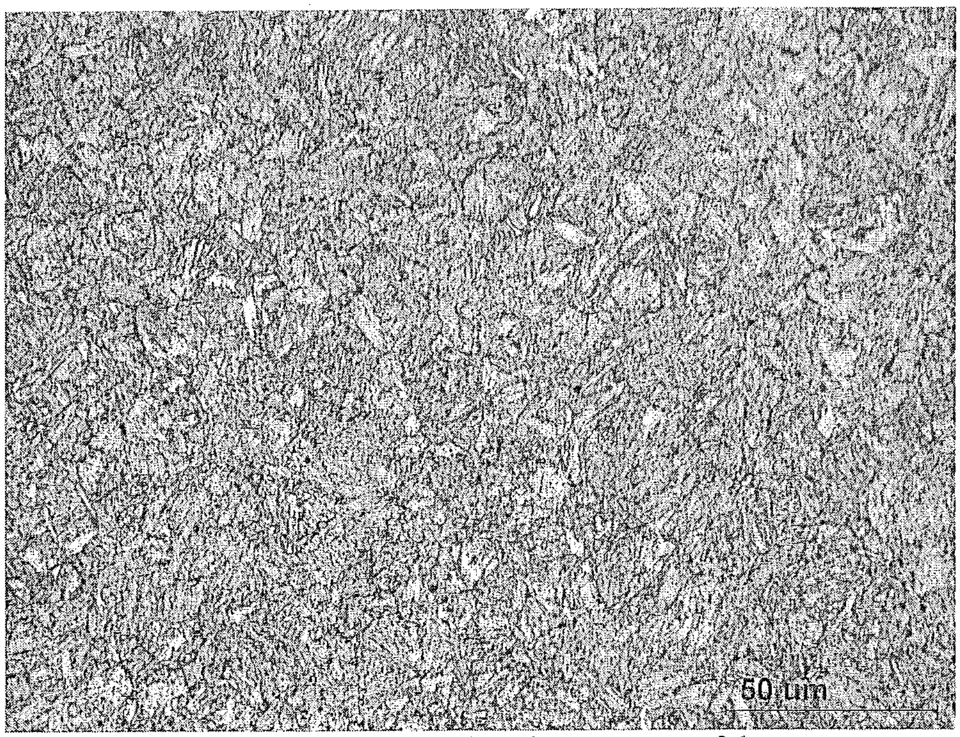

Fig. 9 High magnification showing the microstructure of the transverse section from the gage area.